DEVELOPMENT AND *IN VITRO* CHARACTERIZATION OF POLYMER-BASED NASAL FORMULATIONS OF LEVOTHYROXINE

by

Esomchukwu Vin-Boris Obinna

Submitted in partial fulfilment of the requirements
for the degree of Masters of Science

at

Dalhousie University
Halifax, Nova Scotia
August 2020

TABLE OF CONTENT

LIST OF TABLES…… v

LIST OF FIGURES…… vi

ABSTRACT……x

LIST OF ABBREVIATIONS AND SYMBOLS USED……xi

ACKNOWLEDGEMENTS…….…… xii

CHAPTER 1 INTRODUCTION..... 1

1.1 ANATOMY AND PHYSIOLOGY OF THE THYROID GLAND 1

1.2 DISEASES OF THE THYROID GLAND 2

1.2.1 Hyperthyroidism 2

1.2.2 Hypothyroidism 3

1.3 LEVOTHYROXINE REPLACEMENT THERAPY 4

1.3.1 Chemical and Physical Properties of Levothyroxine 5

1.3.2 Current Levothyroxine Delivery Methods 6

1.4 ANATOMY AND PHYSIOLOGY OF THE NOSE 8

1.5 NASAL DRUG DELIVERY 9

1.5.1 Mechanisms of Nasal Drug Absorption 10

1.5.2 The Rationale for Nasal Mucoadhesive Drug Delivery 11

1.6 EXPERIMENTAL MODELS FOR NASAL DRUG DELIVERY 12

1.6.1 In situ models 12

1.6.2 In vivo models 13

1.6.3 In vitro models 14

CHAPTER 2 OBJECTIVES AND SCOPE 17

CHAPTER 3 MATERIALS AND METHODS 18

3.1 MATERIALS 18

3.2 INSTRUMENTS 18

3.3 CHROMATOGRAPHIC CONDITIONS 19

3.4 HPLC METHOD VALIDATION 20

3.4.1 Linearity and Range 20
3.4.2 HPLC Method Validation: Precision 20
3.4.3 HPLC Method Validation: Accuracy 21
3.4.4 HPLC Method Validation: Limit of Detection and Quantification 21
3.5 Formulation Optimization Studies 21
3.6 Percentage Yield 22
3.7 Percentage Drug Loading 22
3.8 Morphology (Scanning Electron Microscopy) 23
3.9 Particle Size 23
3.10 Zeta Potential Measurements 23
3.11 Differential Scanning Calorimetry (DSC) 24
3.12 Powder X-Ray Diffraction (pXRD) 24
3.13 In vitro Drug Release 24
3.14 Statistical Methods 26

CHAPTER 4 RESULTS 27

4.1 HPLC Validation 27
4.1.1 Linearity 28
4.1.2 Accuracy 29
4.1.3 Precision 29
4.1.4 Limit of detection and limit of quantification 31
4.2 Percentage Yield and Drug Loading 31
4.3 Surface Morphology 33
4.4 Particle Size and Zeta Potential 37
4.5 Differential Scanning Calorimetry (DSC) 38
4.5.1 DSC for Carbopol-Levothyroxine Formulation 38
4.5.2 DSC for Polycarbophil-Levothyroxine Formulation 39
4.5.3 DSC for HPMC-Levothyroxine Formulation 40
4.5.4 DSC for Chitosan-Levothyroxine Formulation 41
4.6 Powder X-Ray Diffraction (pXRD) 42
4.6.1 PXRD for Carbopol-Levothyroxine Formulation 42
4.6.2 PXRD for Polycarbophil-Levothyroxine Formulation 43

4.6.3 PXRD for Levothyroxine-HPMC Formulation 44
4.6.4 PXRD for Levothyroxine-Chitosan Formulation 45
4.7 In vitro Drug Release 46
4.7.1 In vitro Release of Levothyroxine-Carbopol Formulations 46
4.7.2 In vitro Profile of Levothyroxine-Polycarbophil Formulations 47
4.7.3 Invitro Release of Levothyroxine-HPMC Formulations 48
4.7.4 Invitro Release of Levothyroxine-Chitosan Formulations 50
4.8 In vitro Release Kinetics 51
CHAPTER 5 DISCUSSION 53
5.1 Analytical method development and validation 53
5.2 Percentage Yield and Drug Loading 54
5.3 Surface Morphology 55
5.4 Particle Size 55
5.5 Zeta Potential 56
5.6 Differential Scanning Calorimetry (DSC) 57
5.7 Powder X-ray Diffraction 58
5.8 In vitro Drug Release and Kinetics of In vitro Release 58
CHAPTER 6 SUMMARY AND CONCLUSION 61
REFERENCES……..... 62

LIST OF TABLES

Table 1. Physicochemical characteristics of levothyroxine 5

Table 2. Nasal formulations for local and systemic effects. 9

Table 3. Chromatographic conditions for levothyroxine detection 19

Table 4. Accuracy data for 10 µg/ml, 30 µg/ml and 70 µg/ml levothyroxine standard solutions with Varian 920 LC system (n=3). 29

Table 5. Intra-day and inter-day precision for 10 µg/ml, 50 µg/ml, and 100 µg/ml levothyroxine standard solutions with the Varian 920 LC system (n=3). 30

Table 6. Percentage yield and percentage drug loading of levothyroxine-carbopol, levothyroxine-polycarbophil, levothyroxine-HPMC, and levothyroxine-chitosan formulations. 32

Table 7. Particle size and zeta potential of the lyophilized levothyroxine-polymer formulations.. 38

Table 8. Mathematical models for levothyroxine release from carbopol, polycarbophil, HPMC, and chitosan.. 51

LIST OF FIGURES

Figure 1. HPLC chromatogram for 100 µg/ml in acetonitrile and 0.1 % trifluoroacetic acid (70:30) solvent. 27

Figure 2. Linearity of levothyroxine within a concentration range of 0.5-100 µg/ml in acetonitrile and 0.1 % trifluoroacetic acid. 28

Figure 3. Scanning electron images of carbopol 1:1 (A), carbopol 1:3 (B), carbopol 1:5 (C), and raw levothyroxine (D)..... 33

Figure 4. Scanning electron images of polycarbophil 1:1 (A), polycarbophil 1:3 (B), polycarbophil 1:5 (C), mannitol (D) 34

Figure 5. Scanning electron images of HPMC 1:1 (A and B), HPMC 1:3 (C), HPMC 1:5 (D) 35

Figure 6. Scanning electron images of chitosan 1:1 (A and B), chitosan 1:3 (C), chitosan 1:5 (D)..... 36

Figure 7. Differential scanning calorimetry thermograms for raw levothyroxine, carbopol 1:1, carbopol 1:3, and carbopol 1:5. 39

Figure 8. Differential scanning calorimetry thermograms for raw levothyroxine, polycarbophil 1:1, polycarbophil 1:3, and polycarbophil 1:5..... 40

Figure 9. Differential scanning calorimetry thermograms for HPMC 1:1, HPMC 1:3, HPMC 1:5, raw levothyroxine..... 41

Figure 10. Differential scanning calorimetry thermograms for HPMC 1:1, HPMC 1:3, HPMC 1:5, raw levothyroxine..... 42

Figure 11. X-ray diffraction patterns of carbopol 1:1, carbopol 1:3, carbopol 1:5, and raw levothyroxine.. 43

Figure 12. X-ray diffraction patterns of polycarbophil 1:1, polycarbophil 1:3, polycarbophil 1:5, and raw levothyroxine.. 44

Figure 13. X-ray diffraction patterns of HPMC 1:1, HPMC 1:3, HPMC 1:5, and raw levothyroxine.. 45

Figure 14. X-ray diffraction patterns of chitosan 1:1, chitosan 1:3, chitosan 1:5, and raw levothyroxine. 46

Figure 15. *In vitro* cumulative release of levothyroxine from carbopol 1:1, carbopol 1:3, and carbopol 1:5 formulations 47

Figure 16. *In vitro* cumulative release of levothyroxine from polycarbophil 1:1, polycarbophil 1:3, and polycarbophil 1:5 formulations..... 48

Figure 17. *In vitro* cumulative release of levothyroxine from HPMC 1:1, HPMC 1:3, and HPMC 1:5 formulations..... 49

Figure 18. *In vitro* cumulative release of levothyroxine from chitosan 1:1, chitosan 1:3, and chitosan 1:5 formulations..... 50

ABSTRACT

BACKGROUND. Hypothyroidism patients, unable to absorb oral levothyroxine rely on expensive and inconvenient intramuscular injections for life-time hormone replacement. OBJECTIVES: This project aimed to develop a non-invasive, less costly, and patient-friendly nasal delivery alternative using mucoadhesive polymers. METHODS: Nasal formulations were developed with carbopol, polycarbophil, chitosan, and hydroxypropyl methylcellulose (HPMC), respectively. The physicochemical properties and potential for nasal delivery were characterized. RESULTS: The formulation yield was high, with drug loading percentage of 72 -98% and mean particle size of less than 50 µm. The zeta-potential of the powder particles were electronegative and the differential calorimetric analysis and X-ray powder diffraction confirmed drug-polymer integration. The *in vitro* release studies demonstrated sustained levothyroxine release from the polymers over an extended period and their potential for nasal administration. CONCLUSIONS: Results of this study showed that carbopol, polycarbophil, chitosan, and HPMC can be used as sustained-release polymers for intranasal delivery of levothyroxine.

LIST OF ABBREVIATION AND SYMBOLS USED

µg	Microgram
µl	Microlitre
µm	Micrometer
% CV	Percent coefficient of variation
DSC	Differential Scanning Calorimetry
HPLC	High Performance Liquid Chromatography
ICH	International Conference on Harmonization
IM	Intramuscular
IV	Intravenous
LC	Liquid Chromatography
LOD	Limit of Detection
LOQ	Limit of Quantification
R^2	Coefficient of determination
SEM	Scanning electron microscopy
Mg	Milligram
ml	Millilitre
mm	Millimeter
min	Minute
nm	Nanometer
T_3	Triiodothyronine
T_4	Thyroxine
T_m	Melting temperature

T_{onset}	Onset temperature
TRH	Thyroid Releasing Hormone
TSH	Thyroid Simulating Hormone
SCX	Strong Cation Exchange
USP	United State Pharmacopeia

ACKNOWLEDGMENTS

First, all praise goes to God, the creator of all things and giver of wisdom.

I am forever indebted to my mentor and supervisor, Dr. Remigius Agu, for providing me with the opportunity to work and learn in his lab. My co-supervisor, Dr. Syed Ali Imran, provided tremendous expertise and invaluable suggestions throughout the development of this work. I must express special gratitude to Susan Mansour, Director, College of Pharmacy, Dalhousie University. I would also like to thank the College of Pharmacy, Dalhousie University Pharmacy Endowment Fund, and the Faculty of Medicine for funding my education. I immensly appreciate the support of my supervisory committee members, Dr. Tannis Jurgens and Dr. Pollen Yeung, as well as the graduate coordinator, Dr. David Jakeman. The entire administrative staff of the College of Pharmacy, specifically Tracy Jollymore and Wanda Dundas, deserve a lot of credit for helping me whenever I needed assistance. I would also like to acknowledge some of the former students in Dr. Agu's lab that contributed to this project: Ankit Parikh, Anand Utkarshini, Ayah Shakshuki, Arezou Teimouri, Nour Al-Ashi, and Martin Matuvi.

The following labs and individuals deserve a lot of thanks for assisting me with their equipment and expertise: Dr. Rainey's group (Bruce, Jeff, and Andy), Dr. Gagnon's group (Heather), Pat Scallion, and Mike Johnson.

Finally, I would like to thank my family. My heartfelt gratitude goes to my parents who taught me the value of education, hard work, and optimism. My siblings, Jesse and Kenechukwu will always be my inspiration. My partner, Oluwafoyinsayemi Senbanjo, has been my anchor and strength throughout this process. This project is dedicated to her.

CHAPTER 1 INTRODUCTION

1.1 Anatomy and Physiology of The Thyroid Gland

The thyroid gland is the bow-tie shaped tissue located in the lower part of the neck [1]. It lies over the upper portion of the trachea right below the larynx. The gland consists of two lobes connected by a thyroid tissue, the isthmus. The organ is highly vascularized and receives its primary blood supply from the superior thyroid artery and venous drainage from the superior and middle thyroid veins. The thyroid gland's primary function is the production of triiodothyronine (T_3) and thyroxine (T_4). These hormones regulate oxygen consumption, basal metabolic rate, cellular metabolism, and cell growth [2]. Both T_3 and T_4 are amino acid derivatives formed from the addition of iodine to tyrosine in the thyroid gland's follicular cells. The process involves the production and transportation of thyroglobulin from the follicular cells into the colloid, a central cavity filled with a viscous fluid. Iodine from diet is also actively transported by the follicular cells into the colloid. Thyroglobulin serves as a scaffold for iodine attachment to tyrosine. The attachment of one or two iodine molecules to tyrosine leads to monoiodotyrosine (MIT) or diiodotyrosine (DIT), respectively. Both MIT and DIT serve as precursors for T_3 and T_4. An MIT bound to a DIT produces T_3, and two DITs bonded together yields T_4.

After the production of T_3 and T_4, MIT and DIT are stripped of the iodine if they do not form thyroid hormones. Thyroglobulin is then cleaved from T_3 and T_4, and the free thyroid hormones diffuse into the blood. In the plasma, more than 95% of thyroid hormones bind to various proteins such as thyroid-binding globulin, thyroxine-binding prealbumin, and albumin. The most common form of free thyroid hormone in the plasma

is T_4. However, T_3 is more biologically active. The half-life of T_3 is one day, while that of T_4 is 6 - 7 days which explains why T_4 is preferred for hormone replacement.

1.2 Diseases of The Thyroid Gland

1.2.1 Hyperthyroidism

The excessive production of thyroid hormones by the thyroid gland indicates hyperthyroidism. The prevalence of hyperthyroidism is between 0.2 % - 1.3 % in countries that supplement salt with iodine [3]. However, regions without adequate iodization programs have a significantly higher prevalence of hyperthyroidism [4]. The most common method of diagnosing thyroid dysfunction is serum thyroid-stimulating-hormone (TSH) levels assay. TSH in hyperthyroid patients is lower (usually < 0.1 mIU/mL) than the normal range (0.35 - 4.5 mIU/mL). Also, total or free thyroxine is higher in hyperthyroid patients than in normal patients. Graves's disease is the most common cause of hyperthyroidism. It is an autoimmune disease that causes a continuous and excessive production of thyroid hormones. Some of the common symptoms of hyperthyroidism are arrhythmia, increased appetite, weight loss, increased metabolic rate, increased perspiration, and high sensitivity to heat. Graves's disease is usually marked by diffuse goiter, and exophthalmos (bulging of the eyes). The three treatment options for hyperthyroidism are antithyroid drugs, radioactive iodine, and surgery. Thioamide derivatives are the most common compounds used for hyperthyroidism treatment. Propylthiouracil, methimazole, and carbimazole are examples of thioamides. These compounds interfere with the synthesis of the thyroid hormones in the colloid and prevent the production of T_4 and T_3. Radioactive iodine treatment involves the use of iodine-131 (I-131) to shrink the thyroid tissue and limit the amount of thyroid hormone production.

Thyroidectomy involves the surgical removal of a small part of the thyroid gland to prevent T_3 and T_4 production.

1.2.2 Hypothyroidism

Hypothyroidism occurs when the thyroid gland does not produce enough thyroid hormones. It affects 2-5 % of the population in North America [5,6]. The availability of iodine in the diet is an essential predictor of hypothyroidism. In developed or iodine-sufficient countries, Hashimoto's thyroiditis is the leading cause of hypothyroidism. However, in developing countries, iodine deficiency is the leading cause of hypothyroidism. Based on etiology, the three main forms of hypothyroidism are: primary, secondary, and tertiary. Primary hypothyroidism is the most common endocrine dysfunction, and it arises from an abnormality or destruction of the thyroid gland.

Secondary and tertiary hypothyroidism are caused by disorders in the pituitary gland and hypothalamus, respectively. Tumors and inflammatory conditions in the pituitary or hypothalamus can impair thyroid hormone production. Both the pituitary gland and the hypothalamus are integral to the regulation of thyroid hormone synthesis. TSH stimulates the thyroid gland to release T_3 and T_4. Symptoms of hypothyroidism in adults include fatigue, constipation, myxedema, slow metabolic rate, muscle weakness, weak pulse, slow speech, memory loss, cold intolerance, weight gain, and goiter. Hypothyroidism is clinically diagnosed when the serum TSH is above the clinical range (0.35 - 4.5 mIU/mL). Oral replacement therapy with T_4 tablets is the mainstay of hypothyroidism treatment.

1.3 Levothyroxine Replacement Therapy

Levothyroxine is one of the most prescribed drugs in North America, with over a hundred million prescriptions each year [7]. The use of replacement therapy for treating hypothyroidism predates modern medicine. Before discovering thyroid hormone, physicians transplanted whole thyroid glands from animals like sheep and pigs to patients [8]. In 1891, two Portuguese research collaborators, Bettencourt and Serrano, discovered that rather than the gland, thyroid extract, which they described as thyroid juice, was responsible for the benefits observed after transplantation [9]. Three months after their findings, George Murray, an English physician, reported the successful treatment of a myxedema coma patient with thyroid extract injection [10]. After Murray's report, other physicians reported successful treatment of myxedema coma using oral administration of thyroid extracts [11]. Although the isolation of thyroxine was achieved in 1915 by Edward Kendall, the chemical structure was not determined until 1926. Commercial sales of thyroxine tablets did not begin until 1949 [8].

Furthermore, synthetic levothyroxine for human use was not available until 1954. Since 1949, oral thyroxine replacement therapy has been the primary form of treatment for hypothyroidism. In 1997, after nearly 50 years of prescription, the US Food and Drug Administration (FDA) reclassified levothyroxine as a new drug. The reclassification was prompted by a large number of levothyroxine recalls that occurred between 1990 and 1997 [12]. The primary reasons for these recalls were potency and stability issues. Following the action of the FDA, Health Canada conducted a review of all levothyroxine tablets in August 2001. The review did not lead to the discontinuation of any product.

However, in the US, Levothroid (Forest Pharmaceuticals) was banned because it did not meet the FDA's stability requirements.

1.3.1 Chemical and Physical Properties of Levothyroxine

Table 1 shows a summary of the physical and chemical characteristics of levothyroxine important for formulation studies [13]. Levothyroxine has a molecular weight of 776.87 g/mol, water solubility of 0.105 mg/ml, and melting point of 235.5℃. The structure of the drug shows that it is derived from tyrosine and has one chiral centre, four iodine atoms, and two phenol rings.

Table 1. Physicochemical characteristics of levothyroxine

Chemical Name	3,3',5,5'-Tetraiodo-L-thyronine
Molecular Formula	$C_{15}H_{11}I_4NO_4$
Melting Point	235.5℃
Water Solubility	0.105 mg/ml (slightly soluble)
Molecular Weight	776.87 g/mol
logP	4
pKa	0.27 (carboxylic), 7.43 (phenol), 9.34 (amine)
BCS	Class I or Class III
Half-life	7 days

Degradation pathways	deiodination, deamination, and decarboxylation
Chemical Structure	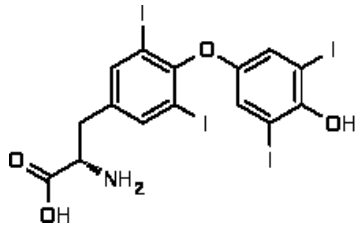

1.3.2 Current Levothyroxine Delivery Methods

Oral and injectable levothyroxine are the two primary dosage forms for thyroid replacement therapy. Synthroid® (BGP Pharma ULC) and Eltroxin® (Aspen Pharmacare Canada Inc.) are the only brands of the drug sold in Canada. In the United States, however, there are five brands: Synthroid (Abbvie, Illinois, USA), Levo-T (Cediprof Inc., Puerto Rico, USA), Unithroid (Stevens J, New York, USA), Levothyroxine Sodium (Mylan, Pensylvania, USA), and Levoxyl (King Pharm, Tennessee, USA). Although most hypothyroid patients can be effectively treated with oral preparations, thyroid hormone management remains challenging in a significant proportion of the patients who have conditions or surgical procedures that affect their gastrointestinal tract. Approximately 60 % - 80% of oral levothyroxine is absorbed in the jejunum and ileum of the small intestine [14]. Besides, levothyroxine absorption is maximal on an empty stomach. As a result, it is common practice for physicians to ask patients to take levothyroxine tablets at least half an hour before breakfast or other medications [15]. However, this strict recommendation can be inconvenient for some patients whose lifestyle or pre-existing conditions do not permit them to delay breakfast.

Furthermore, several conditions and drugs impair thyroxine absorption. Proton-pump inhibitors, antacids, aluminum, magnesium hydroxide, sucralfate, ion exchange resins, and bile acid sequestrants may decrease thyroxine absorption [16]. Besides, several diseases, including celiac disease, atrophic gastritis, *H. pylori* infection, inflammatory bowel disorder, and Crohn's disease, interfere with levothyroxine absorption [17]. Some of the conditions that impair levothyroxine absorption are common in hypothyroidism. Several studies on hypothyroidism have found that patients with Hashimoto's disease are more susceptible to gastrointestinal diseases [18]. Dysfunction in the stomach's parietal cells may contribute to the individual variability observed in daily thyroxine levels of hypothyroid patients [19].

Only Fresenius Kabi, and Avir Pharma market levothyroxine injection in Canada. Both brands have only two dosage options available (200 µg and 500 µg powder vials for reconstitution). In the US, three companies have FDA approval to distribute injectable levothyroxine (Fresenius Kabi USA, Maia Pharms Inc., and Piramal Critical). The dosage options provided by these companies are typically 100 µg, 200 µg, and 500 µg. One of the main difficulties associated with levothyroxine injection is that any unused portion of the drug cannot be stored because it does not contain preservatives. Since injections are mostly available in high doses and cannot be preserved, they are not feasible for patients that require small and regular doses of levothyroxine. Although there are no absorption issues with injectable levothyroxine, it is unpleasant and expensive. Unlike insulin and methotrexate, both of which have self-injectable options, levothyroxine injections require hospital visits and administration by a healthcare professional. Non-invasive delivery via the nasal route may address these issues.

1.4 Anatomy and Physiology of the Nose

The nose has a rich supply of blood from the branches of the internal and external carotid arteries. The external nose is mainly supplied by the facial artery, while the internal nose is supplied by the sphenopalatine and ethmoid arteries. The most prominent features of the external nose are the nostrils, which lie beneath the tip of the nose. The external nose comprises the bony and, cartilaginous framework, deep fibrous connective tissue, adipose tissue, skin, and muscle. The skeletal structure of the nose consists of the frontal bone, nasal bones, and maxilla. The cartilaginous framework, which lies inferior to the nasal bones, includes the alar, septal, and lateral nasal cartilages. These cartilages are responsible for the flexibility of the frontal part of the nose. The external nose is responsible for warming, filtering, and moistening the air that enters the lungs. It is also involved in sensing olfactory stimuli and modifying speech sound. A mucous membrane lines the interior portion of the external nose. The internal part of the nose or the nasal cavity, lies in the skull's anterior part, which is above the oral cavity.

The nasal septum divides the nasal cavity into two equal right and left halves. The nasal cavity has three parts, vestibule, atrium, and respiratory region. The most anterior part of the cavity, the vestibule, is surrounded by cartilage and lined by skin containing hair that prevents dust from entering the internal parts of the nose. In the respiratory region, the superior, middle, and external nasal turbinates each protrude from the lateral wall of the nasal cavity. These turbinates divide the respiratory region into three groove-like passages called superior, middle, and inferior meatus. Mucous membranes line the meatus, and the grooves increase the surface area. The mucous membrane contains blood vessels and pseudostratified ciliated columnar epithelia with several goblet cells. Mucus,

the viscous fluid that lines the nasal epithelial layer, is secreted by the goblet cells. It is composed of water (96%), mucins or glycoproteins (3%), salts (0.5%), and proteins [20]. The main functions of mucus are to protect the nasal epithelium and remove foreign particles from the nasal cavity. The rich blood supply of the nose and its convenient location on the face makes it a suitable organ for drug delivery.

1.5 Nasal Drug Delivery

Nasal drug administration is often used for local (e.g., chronic sinusitis and nasal polyps) or systemic purposes (e.g., immunization and hormone regulation). The effectiveness of the route for systemic outcomes is well documented. Ancient cultures administered herbs and psychoactive plants intranasally for various reasons, including treatment of diseases, spiritual ceremonies, and recreation [21]. Today, the route remains one of the preferred options for systemic and local effects. Intranasal delivery of various therapeutic compounds, including proteins and peptide hormones, has gained a broad interest in academic and commercial laboratories [22–24]. Table 2 shows some drugs marketed in Canada that are available in nasal formulations.

Table 2. Nasal formulations for local and systemic effects.

Product Name	API	Dosage Form	Indications	Target
24 HR Nasal Allergy Relief	Fluticasone propionate	Spray	Allergic rhinitis	Local
Adrenaline Chloride	Epinephrine	Spray	Bronchospasm, bronchial asthmatic paroxysms	Systemic
Decongestant Nose Drop 0.1%	Xylometazoline hydrochloride	Drops	Nasal congestion	Local

Product Name	API	Dosage Form	Indications	Target
Flumist® Quadrivalent	A/H1N1, A/H3N2, B/Victoria, B/Yamagata	Spray	Immunization against influenza	Systemic
Zomig® Nasal Spray	Zolmitriptan	Spray	Migraine	Systemic
Synarel®	Nafarelin acetate	Aerosol	Endometrial pain and lesion	Systemic
Baqsimi®	Glucagon	Powder	Hypoglycemic reaction	Systemic
Nasonex®	Mometasone Furoate	Spray	Allergic rhinitis, nasal polyps	Local
Narcan® Nasal Spray	Naloxone hydrochloride	Spray	Severe respiratory and CNS depression from opioid overdose	Systemic
Apo-Ciclesonide	Ciclesonide	Spray	Allergic rhinitis	Local

1.5.1 Mechanisms of Nasal Drug Absorption

Before contact with the apical side of the nasal epithelium, drug molecules deposited in the nose must first pass through the mucous layer of the nasal mucosa. Studies show that compared to large and charged particles, small, uncharged molecules have higher permeation through this layer of the mucosa [25]. The mucus layer further restricts diffusion of molecules through the mucin, a protein that provides mucus with its viscoelastic property. Diseases and infections can also affect the permeation of molecules by disrupting the temperature and pH of the mucus. Another essential component of nasal drug absorption is the regulation of tight junctions (or zonula occludens). The tight junctions serve as a barrier between the apical and basolateral parts of the epithelia and prevent the diffusion of molecules between cells [26]. However, tight junctions show

variable permeability, which usually depends on the type of cells that form the junction [27,28]. Some compounds, including mucoadhesive polymers, temporarily weaken tight junctions and enhance drug absorption [29,30].

1.5.2 The Rationale for Nasal Mucoadhesive Drug Delivery

Compared to other parenteral delivery routes, the nose is very accessible. It is also a more convenient and comparatively more comfortable way for patients to self-administer drugs than injection. The nasal epithelium is composed of microvilli, which increases its surface area and facilitates the absorption of drug compounds. The highly vascularized epithelium enables drug molecules deposited on its surface to enter the systemic circulation. This mode of direct systemic absorption ensures that hepatic first-pass metabolism is avoided. As a result, drugs can avoid modification or deactivation by gastric and hepatic enzymes. Also, enzymatic activity in the nose is relatively low compared to the GIT. The bioavailability of nasally administered formulations of some drugs is similar to their intravenous alternative [22]. Drugs that require rapid onset (e.g., naloxone) can be effectively delivered through the nose. Furthermore, drugs that require a prolonged or sustained release for systemic effect can be designed using mucoadhesive (or bioadhesive) compounds to achieve optimal therapeutic levels. Mucoadhesive compounds enable drugs to stick to the mucosal surface of a membrane via the formation of hydrogen bonds, hydrophobic interactions, electrostatic interactions, and covalent attachment [31].

Mucociliary clearance removes mucus from the nasal epithelium by the continuous oscillation of the ciliated cells. It protects the nasal cavity from foreign and potentially harmful materials. Dust and other microorganisms trapped in the mucus are expelled by

the clearance system to the nasopharynx and then into the gastrointestinal tract. Under normal conditions, the mucus layer is replaced every 10-15 mins. This rate of replacement is significantly reduced by mucoadhesive polymers [32,33]. In addition, drugs formulated with mucoadhesive polymers can temporarily reduce mucociliary clearance, thereby providing the drug with longer residence time in the nasal cavity [34–36]. The unique characterisitics of a formulation can be determined through experimental investigation. The major models for investigating nasal drug absorption are discussed in the next section.

1.6 EXPERIMENTAL MODELS FOR NASAL DRUG DELIVERY

Pharmaceutical scientists use various models to determine the rate and extent of drug absorption following nasal administration. *In situ*, *in vivo*, and *in vitro* models are used for absorption assessment. *In vitro* models provide the easiest and quickest means to evaluate and predict drug absorption. *In situ* and *in vivo* models, although more expensive, are often preferred in nasal delivery studies because they provide a better understanding of the mechanisms of absorption. Interspecies differences, however, often limit the utility of results from animal studies. Similarly, *in situ* experiments might unavoidably ignore other biological processes and confounds, which might affect drug absorption. Nevertheless, these models provide valuable information about drug absorption. Some features of the three main models are discussed below:

1.6.1 *In situ* models

In situ models refer to the direct perfusion of a drug solution to an intended delivery route in a living animal. The most popular animal models for nasal *in situ* studies

are rats and rabbits [37]. Although the drug delivery experiment is performed using living animals, they are usually anesthetized for the duration of the investigation. The drug solution is often recirculated from a reservoir containing a drug solution to the delivery site. In nasal delivery studies, *in situ* models are essential for understanding the pharmacokinetics of potential drug candidates. Drug absorption estimates can be determined based on the amount of drug in the reservoir after each cycle. While this method uses an intact nasal cavity, several experimental conditions can affect the results. First, the mucus barrier is depleted after a few cycles. This can lead to an overestimation of drug absorption. Also, the speed at which the solution perfuses the nasal tissue can influence absorption and toxicity. Slow perfusion speed increases the residence time of the drug and leads to more prolonged exposure and vice-versa. *In situ* models have been used to demonstrate the transport mechanism of drugs like digoxin and midazolam [38,39].

1.6.2 *In vivo* models

Several factors influence the choice of animal models used in a study. Nasal delivery studies generally use small animals like rats, mice, and guinea pigs for toxicity studies. In contrast, larger animals like rabbits, dogs, and sheep are used for pharmacokinetics and pharmacodynamics studies [40–42]. Differences in the nasal anatomy and histology of animals make results extrapolation from animal studies to humans very challenging. However, the nasal epithelial structure of some animals (e.g. monkey) is similar to that of humans [43].

There are significant ethical concerns on the use of animals for research and drug trials. A commonly employed approach in animal studies is the principle of the 4Rs: replacement, reduction, refinement, and rehabilitation [44]. This principle prioritizes the

welfare of research animals and ensures that they do not endure unnecessary pain or suffering. In nasal drug delivery studies, rabbits are one of the most preferred animal models. Unlike rats and mice, rabbits have the body mass and blood volume that make pharmacodynamics and pharmacokinetics possible [45].

Moreover, rabbits have a larger nasal cavity than smaller animal models, which allow for the administration of large drug doses. Besides, rabbits are relatively cheap and easy to handle compared to sheep and dogs. The nasal and respiratory epithelium of rabbits is composed of pseudo columnar ciliated goblet cells like the human epithelium. Despite the challenges with *in vivo* models, they are still widely employed in drug delivery studies because they offer useful insights into the biopharmaceutical characteristics of therapeutic compounds, which is impossible with any other model.

1.6.3 *In vitro* models

These types of models allow for the compartmental study or isolation of the processes involved in nasal absorption. A unique advantage of *in vitro* models is that confounding variables can easily be controlled. *In vitro* models use either synthetic membranes (e.g., cellulose acetate), excised tissues (primarily from animals dogs, pigs, rabbits, and sheep), or human and animal cell lines to predict the permeation of a formulation [46]. Some examples of cell lines used are RPMI 2650, human nasal tumor cell line, OEPC, a cell line obtained from porcine olfactory tissue, NAS 2BL, a nasal carcinoma cell line derived from rats [47–49]. Absorption studies can be conveniently conducted with cell lines using a diffusion chamber (e.g., Ussing chamber or Franz cells)[50]. Other methods commonly used to determine drug transport include liquid-covered culture and air-interface culture methods. These methods are beneficial in the

early drug development stage when several formulations and iterations are required before a viable drug compound is selected. These models can provide quick feedback on the absorption, metabolism, and toxicity patterns of proposed drug compounds.

1.6.3.1 Kinetics of *in vitro* release

Mathematical models can be used to describe the drug release profile. The main models used to determine release kinetics are zero order, first order, Hixon-Crowell, Higuchi, and Korsmeyer-Peppas. The *in vitro* release tests data are analyzed with the various models, and regression analysis performed to derive a regression coefficient (R^2). The model that produces the highest R^2 indicates the kinetic release pattern. Zero-order kinetics suggests that drug release is independent of drug concentration. Drugs that follow zero-order are released from the formulation excipients at a constant rate over time. Formulations that are designed as reservoir systems follow zero-order kinetics. First-order kinetics follows an exponential release rate that is only dependent on concentration. The graph of a first-order formulation shows a linear relationship between drug release and time. According to the Hixon-Crowell model, the surface area and diameter of the drug matrix is proportional to the cube root of its volume. The Higuchi model describes drug release from a matrix system. The model is based on six assumptions [51]: (1) The drug concentration is much higher than the solubility, (2) The diffusion is unidirectional, (3) The drug thickness is larger than the size of the molecules, (4) The swelling or dissolution is negligible, (5) The diffusion rate is constant, and (6) The optimum sink conditions are achieved in the release media.

The Korsmeyer-Peppas model is used to describe drug release from polymeric systems [52]. This model is used to identify drugs that have more than one release

mechanism. Formulations can also be classified based on diffusion behavior. The main classes are Fickian and non-Fickian. Fickian diffusion describes the movement of molecules from regions of high concentration to areas of low density. If the slope derived from the regression analysis is < 0.5, then the formulation likely conforms to Fickian diffusion. However, if the slope is higher than 0.5 and less than 1, then the spread is non-Fickian. Finally, if the slope is equal to one, the diffusion is considered a zero-order (non-Fickian).

CHAPTER 2 OBJECTIVES AND SCOPE

Currently, the only alternative to oral levothyroxine formulations is intravenous levothyroxine injection. Patients with gastrointestinal disease (e.g., celiac disease, inflammatory bowel disease, ulcerative colitis) or those with gastrointestinal resection cannot adequately absorb orally administered thyroid hormones. These patients are dependent on injections for thyroid hormone replacement. Along with the apparent challenges of injections, like cost and inconvenience, levothyroxine injections are only available in high doses (100 μg - 500 μg). This means that when low doses (e.g. 25 μg) are needed, the rest of the vial is discarded because reconstituted drug cannot be preserved once opened. This is wasteful and expensive over time.

Consequently, levothyroxine injection is not a practical alternative for patients with gastrointestinal dysfunctions that require small and frequent low-dose T_4 replacement therapy. Therefore, the objectives of this study were the following:

1. To develop and optimize lyophilized mucoadhesive powder formulations for the intranasal delivery of thyroid hormone (T_4) using these four mucoadhesive polymers: carbopol, polycarbophil, hydroxypropyl methylcellulose, and chitosan.
2. To characterize the physicochemical properties of the formulations and determine the *in vitro* levothyroxine release profiles from the mucoadhesive powder formulations.

CHAPTER 3 MATERIALS AND METHODS

3.1 Materials

Levothyroxine sodium (Lot: XIBRG-QF) was purchased from TCI America (Portland, OR, USA). Carbopol 971 NF (Lot: 0102083889) and Noveon AA-1 Polycarbophil USP (Lot: 01012046696) samples were provided by IMCD (Brampton, ON, Canada). Hydroxypropyl methylcellulose (Lot: #081M0197V) and chitosan, low molecular weight (Lot: STBH6262) samples were obtained from Sigma-Aldrich (St. Louis, MO, USA). D-mannitol (Lot: WXBC6730V) and Sodium hydroxide (Lot: 45176536) were bought from Sigma-Aldrich (St. Louis, MO, USA) and EMD Chemicals Inc. (Gibbstown, NJ, USA), respectively. HPLC grade methanol (Lot: 187803), trifluoroacetic acid (Lot: A0306506), and HPLC grade acetonitrile (Lot: 191371) were procured from Fisher Scientific (Geel, Belgium), Acros Organics BVBA (Geel, Belgium), and Fisher Scientific (Geel, Belgium), respectively. Deionized water (17.9Ω) was purified in the lab using a Barnstead Nanopure II filtration system.

3.2 Instruments

Liquid chromatography was performed with a Varian 920-LC (Agilent Technologies Inc., Mississauga ON, Canada) with a built-in low-pressure quaternary gradient pump, 50 µl refrigerated autosampler sample loop, UV-Vis detector, and 4-channel degasser. The features of the chromatograms were identified by using the Galaxie chromatography software (Agilent Technologies Inc., Mississauga ON, Canada).

3.3 Chromatographic Conditions

The mobile phase for detecting levothyroxine consisted of acetonitrile and 0.1% TFA (70:30). It was filtered through a 0.22 µm nylon filter (Chromatographic Specialties Inc., ON, Canada) and degassed in an ultrasonic bath sonicator (Branson, CT, USA) for 90 minutes. The pH of the mobile phase was adjusted to 3 using 0.1N HCl. The stationary phase was a Waters Spherisorb® 5 µ SCX 4.6 mm x 250 mm column. The HPLC flow rate was set at 1.0 ml/min, the injection volume was 50 µl, and the detection wavelength was 225 nm.

Table 3. Chromatographic conditions for levothyroxine detection

Column	Waters Spherisorb® 5 µ SCX 4.6 mm x 250 mm column
Mobile Phase	Acetonitrile and 0.1% trifluoroacetic acid (7:3)
pH	3
Flow Rate	1.0 mL/min
Detection	UV-Vis at 225 nm
Injection	50 µl
Run time	10 min

3.4 HPLC Method Validation

3.4.1 Linearity and Range

A standard calibration curve was made using seven calibration points. The calibration range was from 0.5 µg/ml to 100 µg/ml (0.5, 5, 10, 30, 50, 70, and 100 µg/ml). The range was selected based on the expected concentration of levothyroxine in the sample solutions. A graph of concentration (x-axis) against the peak area (y-axis) was plotted, and the linear graph obtained represented the calibration curve. The range was determined by selecting standard solutions where acceptable linearity, accuracy, and precision were obtained.

3.4.2 HPLC Method Validation: Precision

The precision of the method was determined for levothyroxine by analyzing standard samples at three concentrations: 10 µg/ml, 50 µg/ml, and 100 µg/ml. The method was examined for intermediate precision and repeatability. Intra-day precision or repeatability was estimated by injecting the three standard solutions on the same day and calculating the mean percentage coefficient of variation (% CV). Inter-day precision was determined by injecting the standard solutions on three different days and calculating the % CV. The percentage coefficient of variation was accepted if the value was below 5%. Both intra-day and inter-day precision analyses were done using triplicates of the standard solutions.

3.4.3 HPLC Method Validation: Accuracy

Accuracy of the method was determined by analyzing triplicates of 10 µg/ml, 30 µg/ml, and 70 µg/ml standard solutions. The percentage recovery indicated the accuracy of the method.

3.4.4 HPLC Method Validation: Limit of Detection and Quantification

The limit of detection (LOD) and limit of quantification (LOQ) were calculated using the equations below:

$$LOD = (3.3 \times SD) / S$$

$$LOQ = (10 \times SD) / S$$

Where S = slope of the calibration curve and SD = standard deviation of the y-intercept.

3.5 Formulation Optimization Studies

The following polymers were used in this study: carbopol, polycarbophil, HPMC, and chitosan. Drug to polymer ratio for the carbopol, polycarbophil, HPMC, and chitosan formulations were 1:1, 1:3, and 1:5. The literature on drug-polymer formulations are replete with various ratio combinations. Notwithstanding, the ratio variation selected in this study was based on a review of the literature on nasal mucoadhesive formulations which involved different active pharmaceuticals. The 1:1, 1:3, 1:5 ratios seemed to be the most employed, because these variation accounted for different levels (equal, medium, high polymer content) of polymers and also maintained the quantity of the formulation to an amount suitable for nasal administration [53–55]. Each formulation was developed by adding levothyroxine and the appropriate ratio of one type of mucoadhesive polymer. The

compounds were then triturated with a mortar and pestle. The homogenous triturant was dissolved in 0.01 M methanolic NaOH and sonicated for 30 minutes. D-mannitol (bulking agent and cryoprotectant) was dispersed in deionized water and sonicated for 30 minutes [56]. The levothyroxine-polymer solution was then pipetted into the D-mannitol solution. The mixture of levothyroxine-polymer and D-mannitol was sonicated for 30 minutes and frozen at -80°C for at least 24 hours before lyophilization (freeze-drying). The product recovered after lyophilization was micronized with a 250 μm sieve and stored at -23°C.

3.6 Percentage Yield

The percentage yield of each formulation was calculated as the weight of the final product after freeze-drying relative to the weight before lyophilization [57]. The formula below was used to obtain the percentage yield:

$$\%\ \boldsymbol{Yield} = \frac{\boldsymbol{Weight\ after\ lyophilization}}{\boldsymbol{Weight\ before\ lyophilization}} \times \mathbf{100}$$

3.7 Percentage Drug Loading

Drug loading was determined by dissolving an equal amount of each formulation in 10 ml of methanolic NaOH. The solution was then injected into the HPLC for analysis. The drug concentration in each formulation was determined using the levothyroxine standard curve. Percentage of drug loading was calculated using the equation below:

$$\%\ \boldsymbol{Drug\ loading} = \frac{\boldsymbol{Actual\ drug\ content}}{\boldsymbol{Theoretical\ drug\ content}} \times \mathbf{100}$$

3.8 Morphology (Scanning Electron Microscopy)

The morphology of the samples was examined using a Hitachi S-4700 Scan Electron Microscope (SEM). Each formulation was mounted on an aluminum specimen stub with the aid of a conductive liquid silver adhesive paste. The paste was left to dry overnight, and the stubs with the samples were stored in a fridge. The particles were analyzed at 1.5 kV acceleration, and magnification was between 100x and 2500x. Representative electron microscopic images were obtained.

3.9 Particle Size

The size of the formulations was determined by dispersing 5 mg of each formulation in 2 ml of deionized water. The dispersion was transferred into a cuvette, and a Nano-ZS Zetasizer (Malvern Panalytical Ltd., Malvern Worcestershire, UK) was used to determine the size of the particles in the formulation. Measurement was performed in triplicates, and the Zetasizer software was used to analyze the formulations.

3.10 Zeta Potential Measurements

The zeta potential of the formulations was determined by dispersing 5 mg of each formulation in 5 ml of deionized water. The dispersion was transferred into a zeta cell, and a Nano-ZS Zetasizer (Malvern Panalytical Ltd., Malvern Worcestershire, UK) was used to determine the charge of the formulation. Measurements were performed in triplicates. The Zetasizer software was used to analyze the formulations.

3.11 Differential Scanning Calorimetry (DSC)

The thermogram of each formulation was recorded using a TA Instruments Q200 differential scanning calorimeter (DSC, TA Instruments, DE, USA) equipped with a liquid nitrogen cooling accessory. Samples were prepared by adding 5 mg - 10 mg of a formulation to a tared sample pan (Perkin Elmer hermetic pans) and the mass recorded. The weighed sample was then hermetically sealed with the appropriate press (Perkin Elmer tool). The samples were analyzed over the temperature range of -100 °C to 300 °C at a scanning rate of 10 °C min^{-1} under a helium flow rate of 25 ml min^{-1}.

3.12 Powder X-Ray Diffraction (pXRD)

PXRD was conducted to determine the bond structure of the formulations. X-ray diffraction patterns were measured with a Bruker Advance D8 (Brucker, Massachusetts, United States). A Cu-K_a source (1.00 Å) operating at 40 kV and 30 mA was used to produce the X-rays that were subsequently detected with a scintillation detector (Brucker, Massachusetts, United States). X-ray data were acquired over 10 - 70 2θ degrees in 0.05° increments and a dwell time of 3 seconds. Test samples were prepared by filling sample fixture wells with powder formulations and compacting them with a glass slide to produce smooth surfaces.

3.13 In vitro Drug Release

The *in vitro* drug release study was performed using a six- celled Franz diffusion system with a 5 ml receptor volume and 0.64 cm^2 diffusion aperture. The Lauda Ecoline

water bath circulator maintained the temperature of the Franz cells at 25 ± 0.5 °C. Before each experiment, the system equilibrated for one hour. The receptor fluid, 0.01 M methanolic sodium hydroxide, was prepared by dissolving 400 mg of sodium hydroxide in 500 ml of water after the solution cooled, 500 ml of methanol was added to the NaOH solution. The receptor fluid was degassed using the Branson Ultrasonic bath for 1 hour and donor membrane consisting of course cellulose membrane was hydrated in the receptor fluid for 45 minutes. The receptor fluid was stirred continuously in the Franz cell at 650 RPM using the small magnetic stirrer. The donor chamber of each cell was gradually filled with the receptor fluid using a 5-ml pipette. The hydrated membrane and Teflon O-ring were gently placed over the diffusion aperture to avoid bubbles. After applying 15 mg of the formulation on the membrane, the donor chamber was carefully placed on the O-ring. The receptor chamber was fastened to the donor chamber using the pinch clamp, and a piece of Parafilm was used to cover the top of the donor chamber. Each Franz cell's sampling port was covered with an improvised seal made with aluminum foil and Parafilm. Throughout the release study, the entire Franz diffusion system was covered with a sheet of aluminum foil.

Samples were withdrawn from the receptor chamber at different time intervals over 4 hours (0.5, 1, 1.5, 2, 3, 4 hours). The volume of samples withdrawn at each time point was 0.5 ml. A micropipette and flexible PermGear pipette tip were used to remove samples from the receptor chamber. After removing a specimen, an equal volume (0.5 ml) of fresh receptor fluid was added to the receptor chamber. This was done to maintain sink conditions and receptor fluid-membrane contact. The samples were stored in a 6 °C

refrigerator for analysis the next day. The release for each formulation was conducted in triplicates. Mean cumulative release (%) was obtained using the equation:

$$\text{Cumulative Release (\%)} = (Vs/Vf) \times P(t-1) + Pt$$

Where Vs.: volume of withdrawn sample, Vf: volume of Franz diffusion cell, Pt: percentage release at time t, and P(t-1): percentage release at the previous time 't.'

3.14 Statistical Methods

Data obtained in this study were reported as mean ± SD (n=3). Statistical analysis was done using GraphPad-Prism 5.01 software (San Diego, CA, USA); the difference between the percentage yield, percentage drug load, particle size, zeta potential, and *in vitro* drug release was determined by two-way ANOVA and Bonferroni post-hoc test. Statistical significance was determined at $p < 0.05$.

CHAPTER 4 RESULTS

4.1 HPLC Validation

HPLC validation was conducted to determine the accuracy and reliability of levothyroxine analyses. The parameters for detection and quantification used in this study was based on already established in-house protocol (Table 3). The mobile phase for the analysis was acetonitrile and 0.1 % trifluoroacetic acid (70:30). The stationary phase was a silica Spherisorb® column. Figure 1 is a chromatogram that shows the detection of 100 µg/ml concentration of levothyroxine in a 50 µl solution. The run and retention time of the drug was 10 minutes and 4.6 minutes, respectively.

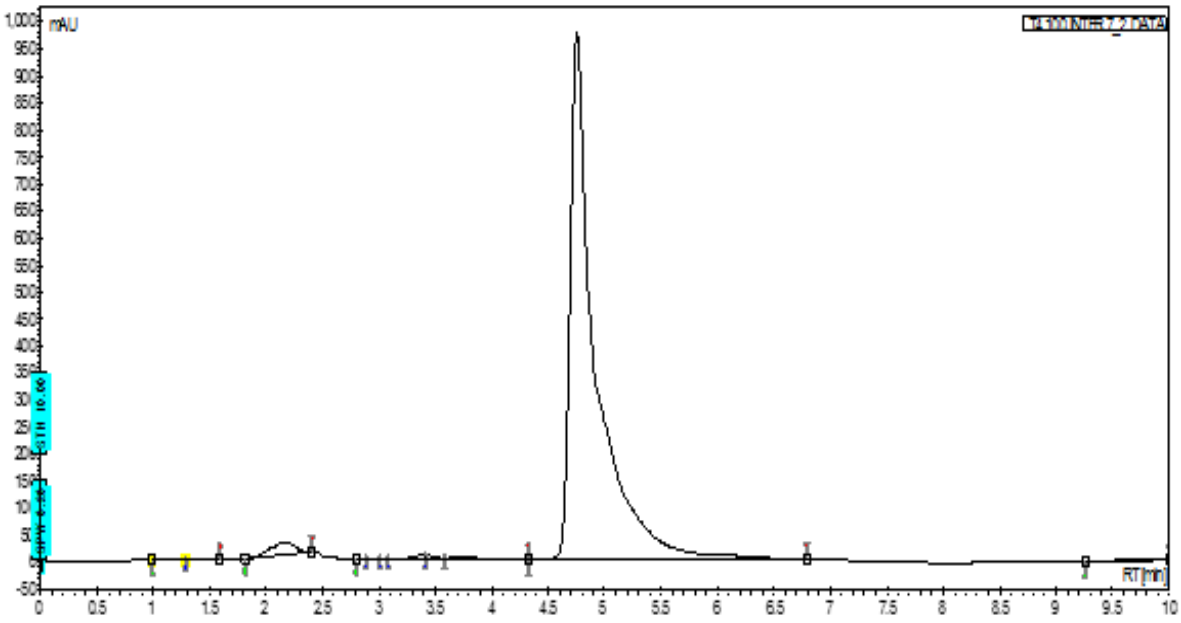

Figure 1. HPLC chromatogram for 100 µg/ml in acetonitrile and 0.1 % trifluoroacetic acid (70:30) solvent.

4.1.1 Linearity

After validating the analytical instrument, the linearity was determined using 0.5, 5, 10, 30, 50, 70, and 100 µg/ml levothyroxine standard solutions. A calibration curve of concentration against the area under the curve obtained from the HPLC was plotted. A linear trend line was observed between the variables (Figure 2). The coefficient of determination (R^2) was 0.9992, and the equation for the trend line was y = 2.483x + 2.1513. The range of linearity was determined based on the expected concertation of levothyroxine in the samples during the experiments.

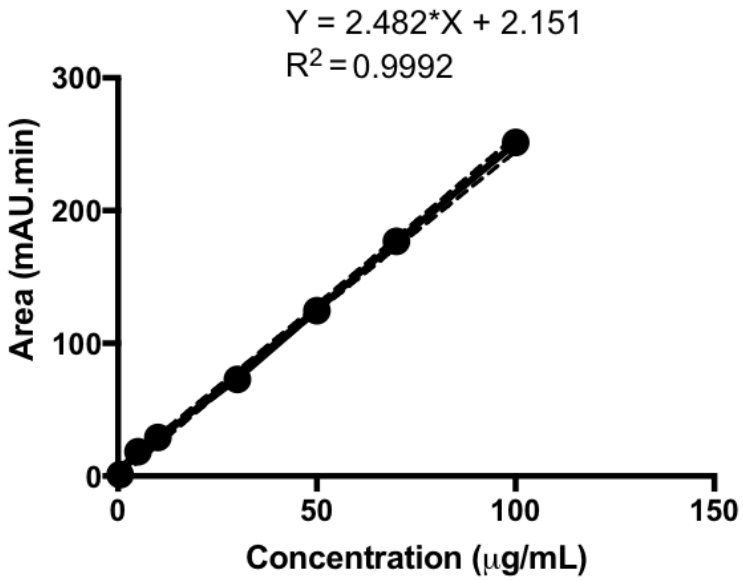

Figure 2. Linearity of levothyroxine within a concentration range of 0.5-100 µg/ml in acetonitrile and 0.1 % trifluoroacetic acid.

4.1.2 Accuracy

The accuracy was determined across the linear analytical range specified for levothyroxine. The data obtained are summarized in Table 4. The percentage recovery of the standard samples was within acceptable ICH guidelines of 95 % -1 00 % [58].

Table 4. Accuracy data for 10 µg/ml, 30 µg/ml and 70 µg/ml levothyroxine standard solutions with Varian 920 LC system (n=3).

Concentration	**10 µg/ml**	**30 µg/ml**	**70 µg/ml**
Amount Recovered µg/ml	9.5 9.5 9.6	28.5 29.7 29.8	70.3 71.3 71.5
Mean	9.5	29.3	71.0
Standard Deviation	0.1	0.7	0.6
% RSD	0.6	2.5	0.9
% Recovery	95.3	97.8	101.5

4.1.3 Precision

In the precision studies, the mean percentage coefficient of variation for the standard samples, 10 µg/ml, 50 µg/ml, and 100 µg/ml was 0.20 %, 1.49 %, and 1.04 %, respectively. The mean % CV for inter-day analysis was 0.91%. All results obtained were within the acceptable limit of 5%. The precision data are summarized in Table 5

Table 5. Intra-day and inter-day precision for 10 µg/ml, 50 µg/ml, and 100 µg/ml levothyroxine standard solutions with the Varian 920 LC system (n=3).

		Conc. (µg/ml)	Intra-day Precision			Inter-day Precision		
			Mean	SD	CV (%)	Mean	SD	CV (%)
Standard 10 µg/ml	**Day 1**	9.5 9.4 9.3	9.4	0.1	1.1	9.42	0.02	0.20
	Day 2	9.5 9.4 9.4	9.4	0.1	0.6			
	Day 3	9.2 9.5 9.6	9.4	0.2	2.2			
Standard 50 µg/ml	**Day 1**	49.3 49.7 48.4	49.1	0.7	1.4	49.10	0.73	1.49
	Day 2	49.9 49.9 49.8	49.9	0.1	0.1			
	Day 3	48.8 48.4 48.0	48.4	0.4	0.8			
Standard 100 µg/ml	**Day 1**	100.3 101.8 100.1	100.7	0.9	0.9	100.02	1.04	1.04
	Day 2	100.2 100.4 100.9	100.5	0.4	0.4			
	Day 3	99.0 99.0 98.5	98.3	0.3	0.3			

4.1.4 Limit of detection and limit of quantification

The limit of detection (LOD) is the lowest concentration of analyte in a sample that can be detected by the HPLC but not accurately quantified. Similarly, the limit of quantification (LOQ) is the minimum concentration at which the HPLC can reliably detect the analyte in an unknown sample. These parameters describe the sensitivity of the HPLC and were derived using Equation 1 and Equation 2, according to the ICH guidelines. LOD and LOQ for levothyroxine analysis were 5.8 µg/ml and 17.8 µg/ml, respectively. Both concentrations were sufficiently below the expected quantity of levothyroxine in this study. Therefore, the HPLC was a suitable instrument for levothyroxine analysis.

LOD = (3.3 x SD) ÷ S…...Equation 1

LOQ = (10 x SD) ÷ S…...Equation 2

Where S = slope of the calibration curve, and SD = standard deviation of the y-intercept.

4.2 Percentage Yield and Drug Loading

The percentage yield and percentage drug load for the carbopol, polycarbophil, HPMC, and chitosan formulations are shown in Table 6. The percentage yield for the carbopol formulations was between 98 – 100 %. The amount of levothyroxine loaded into the carbopol formulation for the 1:1, 1:3, and 1:5 formulations was 80.7 ± 2.1 %, 90.0 ± 1.7 %, and 87.3 ± 2.1 %, respectively. The polycarbophil formulations had a percent yield between 99 % and 102 %. The levothyroxine content of the polycarbophil

formulation 1:1, 1:3, and 1:5 was 101.1 ±2.3 %, 99.8 ± 1.4, and 99.5 ± 2.1 %, respectively. The HPMC formulations yielded between 100 % - 102 %. The percent drug loaded for HPMC 1:1, 1:3, and 1:5 was 72%, 95%, and 84%, respectively. The three chitosan formulations had percentage yield between 99% and 102%, and the amount of levothyroxine loaded was 88.7 ± 8.0 %, 92.7 ± 7.6 %, and 98.0 ± 3.5 % for the 1:1, 1:3, and 1:5 formulations, respectively.

Table 6. Percentage yield and percentage drug loading of levothyroxine-carbopol, levothyroxine-polycarbophil, levothyroxine-HPMC, and levothyroxine-chitosan formulations. The data are presented as mean ± SD (n=3).

Formulation code	**Percentage yield (%)**	**Drug loading (%)**
Carbopol 1:1	100.7 ± 1.3	80.7 ± 2.1
Carbopol 1:3	98.3 ± 0.5	90.0 ± 1.7
Carbopol 1:5	98.0 ± 1.4	87.3 ± 2.1
Polycarbophil 1:1	101.1 ±2.3	91.3 ± 1.5
Polycarbophil 1:3	99.8 ± 1.4	76.0 ± 2.6
Polycarbophil 1:5	99.5 ± 2.1	79.3 ± 1.5
HPMC 1:1	100.0 ± 0.8	72.0 ± 5.3
HPMC 1:3	102.0 ± 0.6	94.6 ± 9.0
HPMC 1:5	100.2 ± 0.3	84.0 ± 7.0
Chitosan 1:1	99.6 ± 0.5	88.7 ± 8.0
Chitosan 1:3	101.1 ± 0.3	92.7 ± 7.6
Chitosan 1:5	102.0 ± 0.1	98.0 ± 3.5

4.3 Surface Morphology

Surface roughness is important in lyophilized products because it increases the contact angle and wettability of the particles [59]. Scan Electron Microscopy (SEM) was used to examine the surface morphology of the formulations, because of its high image resolution. The images in Figure 3 show the surface morphology of the carbopol formulations and raw levothyroxine. The carbopol formulations all had a rough surface morphology with an uneven appearance. Levothyroxine (Figure 3D) exhibited a coarse surface morphology.

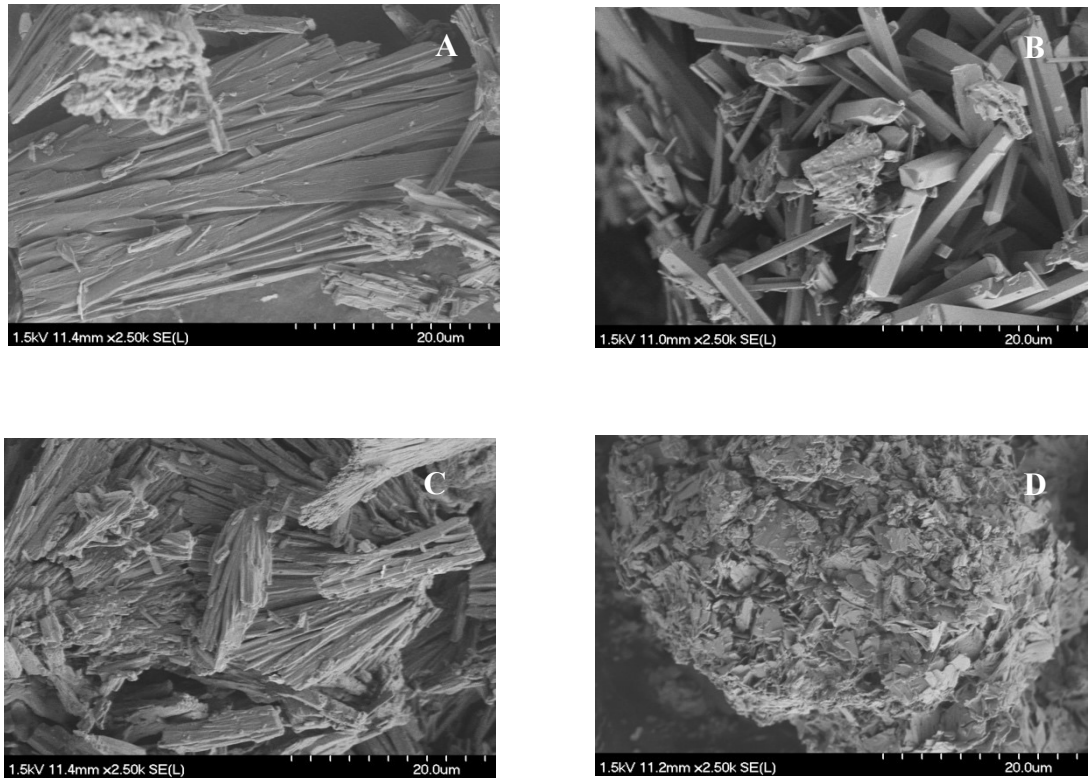

Figure 3. Scanning electron images of carbopol 1:1 (A), carbopol 1:3 (B), carbopol 1:5 (C), and raw levothyroxine (D). Each sample was mounted with the aid of a conductive silver adhesive paste and particles were analyzed at 1.5 kV acceleration, and 20.0 μm magnification.

SEM images of the polycarbophil formulations and mannitol were obtained to study their surface morphology. Figure 4 shows that the polycarbophil formulations had a rough and porous suface appearance. Mannitol, the main excipient in all the formulations, had an irregular and uneven surface morphology (Figure 4D).

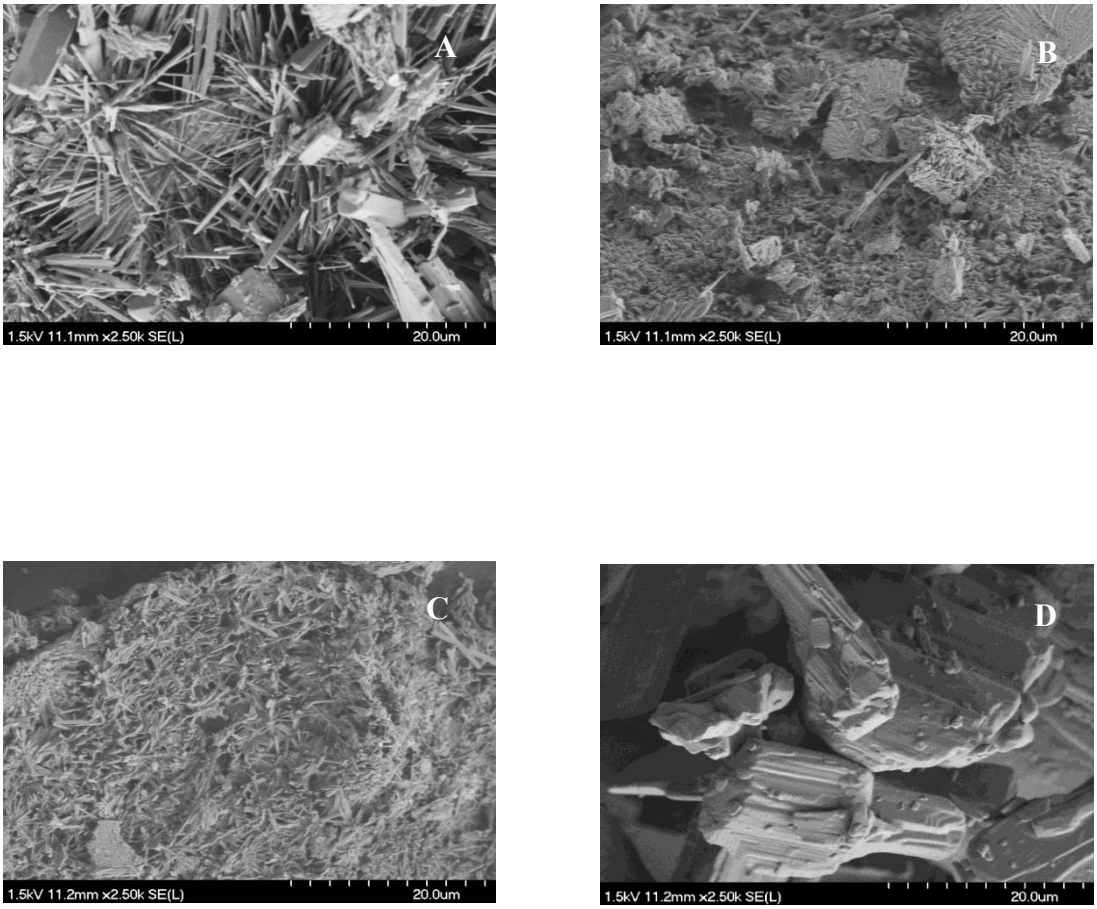

Figure 4. Scanning electron images of polycarbophil 1:1 (A), polycarbophil 1:3 (B), polycarbophil 1:5 (C), mannitol (D). Each formulation was mounted with the aid of a conductive silver adhesive paste and particles were analyzed at 1.5 kV acceleration, and magnification set at 20.0 μm.

The surface morphology of the HPMC formulations were analyzed with SEM. Not only is the surface of the HPMC formulations rough and porous, the powder particles have a distict needle-like appearance (Figure 5). The shape and appearance of the particles indicate crystallization which occurred during lyophilization.

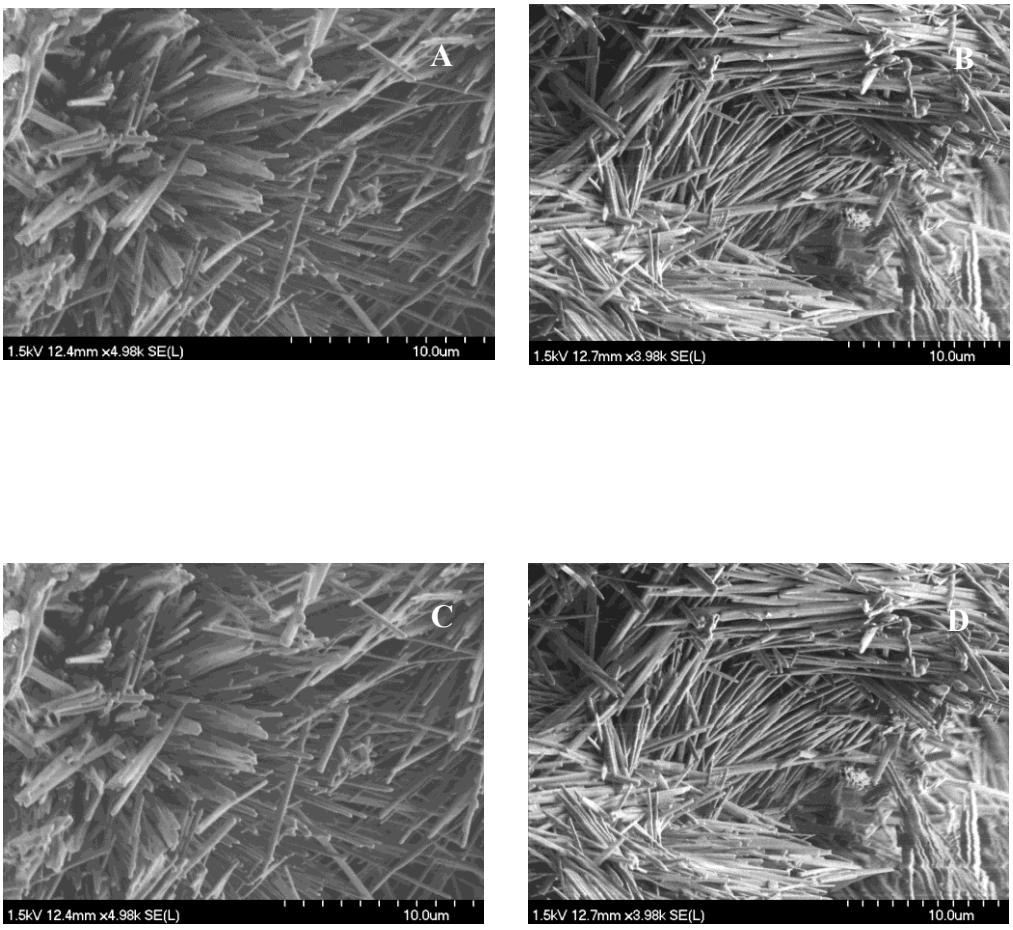

Figure 5. Scanning electron images of HPMC 1:1 (A and B), HPMC 1:3 (C), HPMC 1:5 (D). Each formulation was mounted with the aid of a conductive silver adhesive paste and particles were analyzed at 1.5 kV acceleration, and magnification was set at 10.0 μm.

The images in Figure 6 show the surface morphology of the chitosan formulations. These formulations had a rough and layered surface morphology. Similar to the HPMC formulations, chitosan particles had a needle-like appearance. However, the arrangement of the chitosan particles were more compact than HPMC particles.

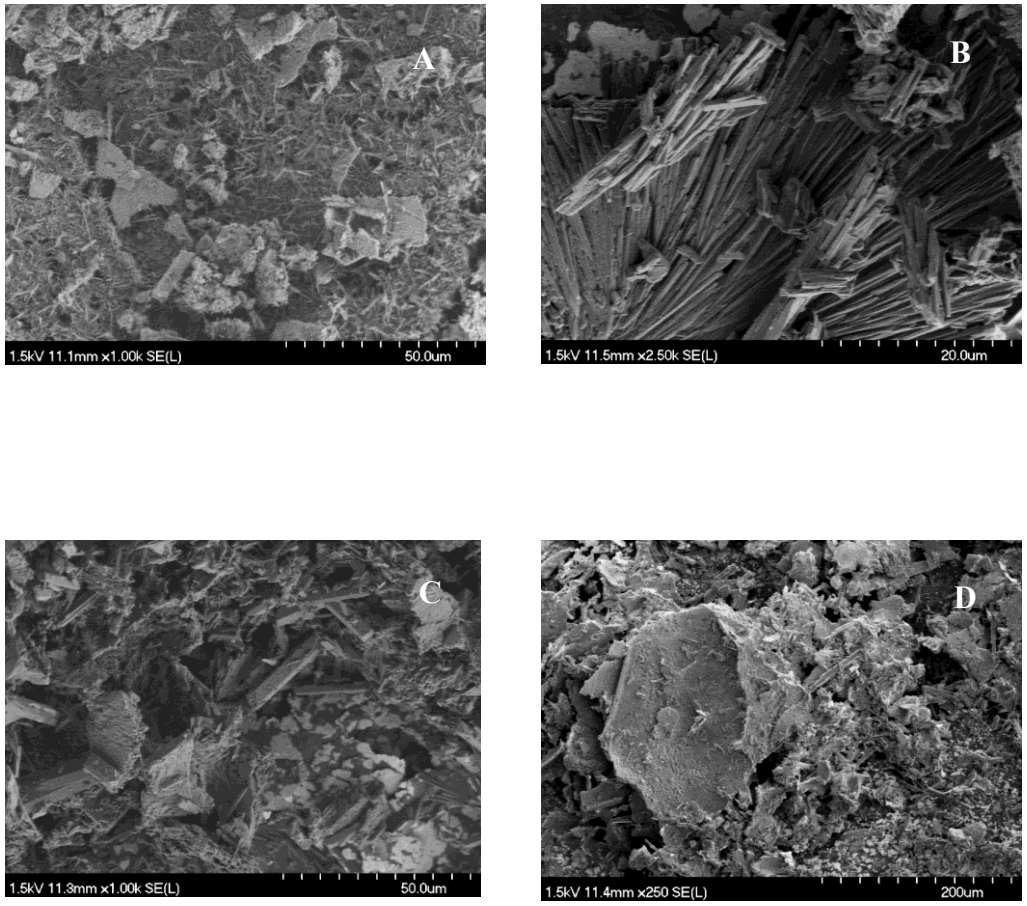

Figure 6. Scanning electron images of chitosan 1:1 (A and B), chitosan 1:3 (C), chitosan 1:5 (D). Each formulation was mounted with the aid of a conductive silver adhesive paste and particles were analyzed at 1.5 kV acceleration, and magnification was between 10.0 μm and 200.0 μm.

4.4 Particle Size and Zeta Potential

The particle size and zeta potential of the formulations were measured with a Zetasizer. Table 7 shows the mean particle size and mean zeta potential for the formulations. The range of particle size for the carbopol formulation was between 2.6 μm and 51.9 μm. The mean particle size for the polycarbophil 1:1 formulation was 10.8 ± 0.4 μm, polycarbophil 1:3 particles measured 14.0 ± 1.5 μm, and the polycarbophil 1:5 had a size of 46.9 ± 6.5 μm. The HPMC formulations showed a smaller particle size compared to carbopol and polycarbophil formulations. The mean particle size of the HPMC 1:1 formulation was 0.56 ± 0.02 μm. The range for the mean particle size of the chitosan formulations was between 0.42 μm and 4.14 μm. Carbopol and polycarbophil formulations showed a significant difference in particle size as the ratio of polymer increased (two-way ANOVA: $p<0.05$). However, an increase in polymer did not lead to a significant difference in the particle size of the HPMC and chitosan formulations (two-way ANOVA: $p>0.05$). Although all formulations showed negative zeta potential, the carbopol formulations were the most electronegative. The zeta potential of the carbopol 1:1, 1:3, and 1:5 formulation was - 52.4 ± 2.6 mV, - 58.0 ± 2.0 mV, and - 55.5 ± 1.3 mV, respectively. HPMC formulations were the least electronegativity. HPMC 1:1,1:3, and 1:5 had a zeta potential of -11.66 ± 3.16 mV, -6.06 ± 3.92 mV, and -6.06 ± 1.68 mV.

Table 7. Particle size and zeta potential of the lyophilized levothyroxine-polymer formulations. The measurements were recorded using a Zetasizer. The data are presented as mean ± SD (n=3).

Formulation code	Size (μm)	Zeta potential (mV)
Carbopol 1:1	2.9 ± 0.3	- 52.4 ± 2.6
Carbopol 1:3	19.0 ± 5.7	- 58.0 ± 2.0
Carbopol 1:5	44.2 ± 7.7	- 55.5 ± 1.3
Polycarbophil 1:1	10.8 ± 0.4	- 40.5 ± 1.9
Polycarbophil 1:3	14.0 ± 1.5	- 47.4 ± 2.5
Polycarbophil 1:5	46.9 ± 6.5	- 53.6 ± 3.0
HPMC 1:1	0.56 ± 0.02	-11.66 ± 3.16
HPMC 1:3	0.22 ± 0.06	-6.06 ± 3.92
HPMC 1:5	0.46 ± 0.04	-6.06 ± 1.68
Chitosan 1:1	2.45 ± 0.88	-18.70 ± 1.00
Chitosan 1:3	2.76 ± 1.38	-16.20 ± 0.79
Chitosan 1:5	1.59 ± 0.27	-19.17 ± 1.01

4.5 Differential Scanning Calorimetry (DSC)

4.5.1 DSC for Carbopol-Levothyroxine Formulation

The melting temperature (T_m), which is the point where the endothermic peak appeared, was 131.3 ℃ for the carbopol 1:1 formulation (Figure 7). The onset temperature (T_{onset}) is the extrapolated tangent that marks the beginning of melting. T_{onset} for the carbopol 1:1 formulation was 115.6 ℃. The energy required for a phase change to occur in carbopol 1:1 (ΔH) was 267.4 J/g. The T_{onset}, T_m, and ΔH for the carbopol 1:3 formulation was 125.6 ℃, 132.2 ℃, and 257.3 J/g, respectively. The carbopol 1:5 formulation had a T_{onset} at 123.9 ℃, T_m at 130.9 ℃, and ΔH of 252.4 J/g. Levothyroxine

powder had a much lower endothermic peak with a ΔH of 93 J/g. Although the T_{onset} of levothyroxine occurred at 108.6 ℃, a more significant temperature change was required for melting (T_m = 149.3 ℃) compared to the formulations.

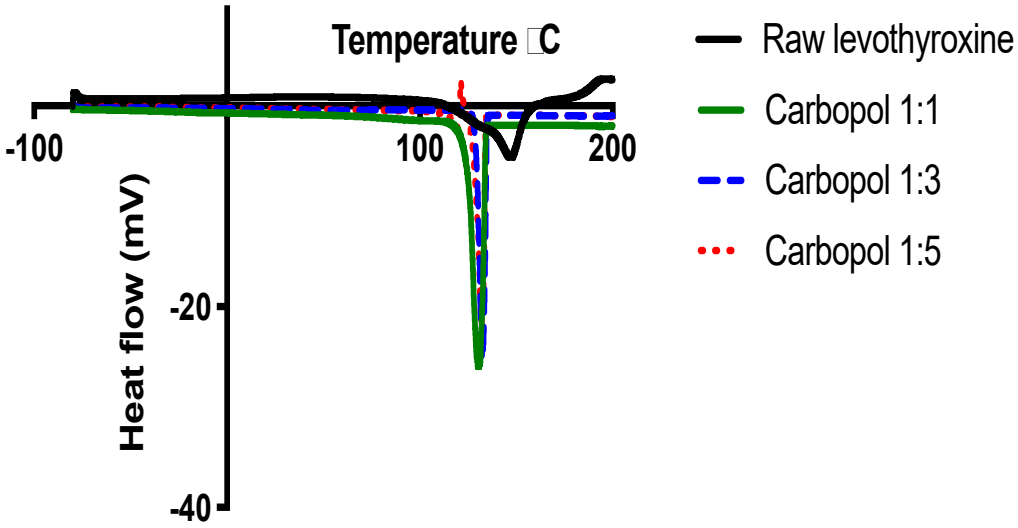

Figure 7. Differential scanning calorimetry thermograms for raw levothyroxine, carbopol 1:1, carbopol 1:3, and carbopol 1:5. The samples were analyzed over the temperature range -100 °C to 300 °C.

4.5.2 DSC for Polycarbophil-Levothyroxine Formulation

The T_{onset} for polycarbophil 1:1 formulation was 125.8 ℃, and the T_m was 132.4 ℃. The ΔH obtained for the polycarbophil 1:1 was 233.4 J/g (Figure 8). The polycarbophil 1:3 formulation showed a T_{onset}, T_m, and ΔH of 127.9 ℃, 132.7 ℃, and 215.1 J/g. The polycarbophil 1:5 formulation had a T_{onset} of 125.9 ℃ and T_m of 132.7 ℃. The ΔH for polycarbophil 1:5 was 200.3 J/g.

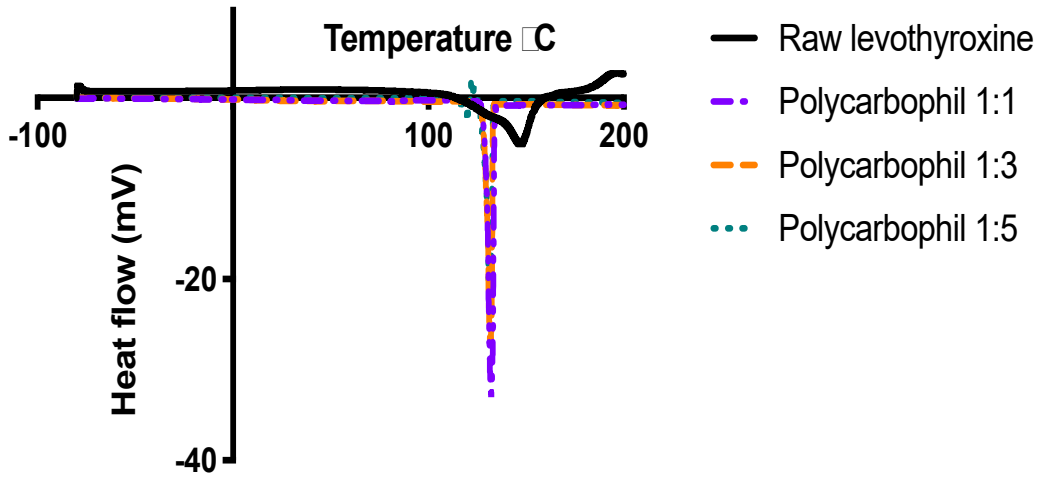

Figure 8. Differential scanning calorimetry thermograms for raw levothyroxine, polycarbophil 1:1, polycarbophil 1:3, and polycarbophil 1:5. The samples were analyzed over the temperature range -100 °C to 200 °C.

4.5.3 DSC for HPMC-Levothyroxine Formulation

The thermal characterisitics of the HPMC formulations are shown in the thermogram below (Figure 9). The HPMC 1:1 formulation showed a T_{onset}, T_m, and ΔH of 164.6 °C, 168.5 °C, and 317.7 J/g. The T_{onset} for the 1:3 formulation was 163.9 °C, and the T_m was 169.8 °C. The ΔH obtained from the HPMC 1:3 was 299.8 J/g. The HPMC 1:5 formulation showed T_{onset} of 164.0 °C, T_m of 169.7 °C, and ΔH was 293.7 J/g.

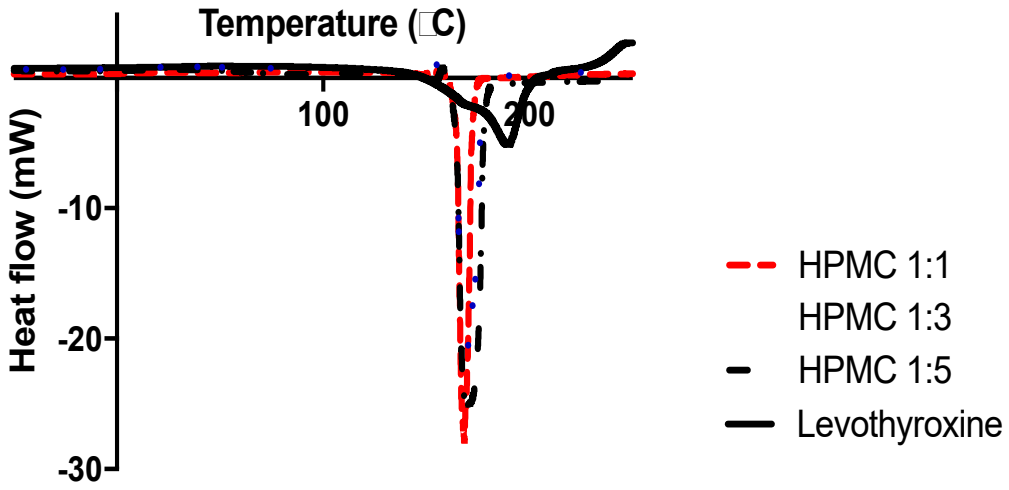

Figure 9. Differential scanning calorimetry thermograms for HPMC 1:1, HPMC 1:3, HPMC 1:5, raw levothyroxine. The samples were analyzed over the temperature range -100 °C to 300 °C at a scanning rate of 10 °C min-1 under a helium flow rate of 25 ml min^{-1}. All the samples had endothermic peaks between 100 °C and 250 °C.

4.5.4 DSC for Chitosan-Levothyroxine Formulation

The ΔH obtained from the chitosan 1:1 was 321.6 J/g. T_{onset} for carbopol 1:1 formulation was 164.9 ℃ and the T_m was 167.0 ℃ (Figure 10). The chitosan 1:3 formulation had a T_{onset}, T_m, and ΔH of 165.9 ℃, 167.4 ℃, and 312.0 J/g. The chitosan 1:5 formulation had a T_{onset} of 167.4 ℃ and T_m of 167.9 ℃. The ΔH obtained for chitosan 1:5 was 305.9 J/g.

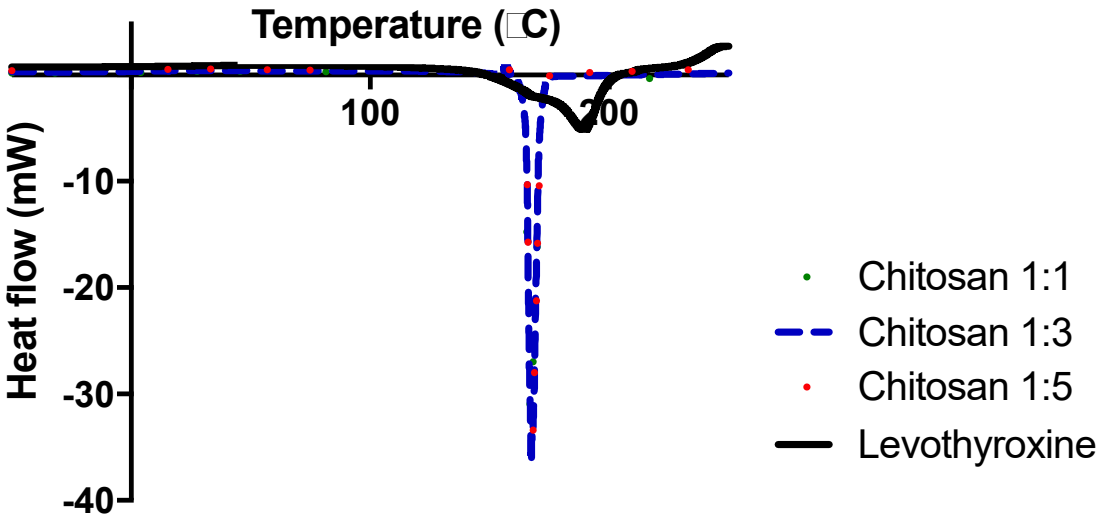

Figure 10. Differential scanning calorimetry thermograms for HPMC 1:1, HPMC 1:3, HPMC 1:5, raw levothyroxine. The samples were analyzed over the temperature range -100 °C to 250 °C.

4.6 Powder X-Ray Diffraction (pXRD)

4.6.1 PXRD for Carbopol-Levothyroxine Formulation

Figure 11 shows the undifferentiated peaks of raw levothyroxine between 20° and 40°. Conversly, The carbopol 1:1 formulation showed five major (differentiated) peaks at 14.5°, 19.3°, 20.9°, 24.5°, and 30°; the minor peaks occurred at 38.0°and 44.0°. The major peak observed for carbopol 1:3 was at 20.3°. The minor peaks for the carbopol 1:3 formulations appeared at 17.1°, 40.7°, and 45.1°. Carbopol 1:5 had five major peaks which occurred at 21.0°, 22.3°, 22.6°, 24.6°, and 28°. The two minor peaks for carbopol 1:5 were at 36.0° and 40.6°.

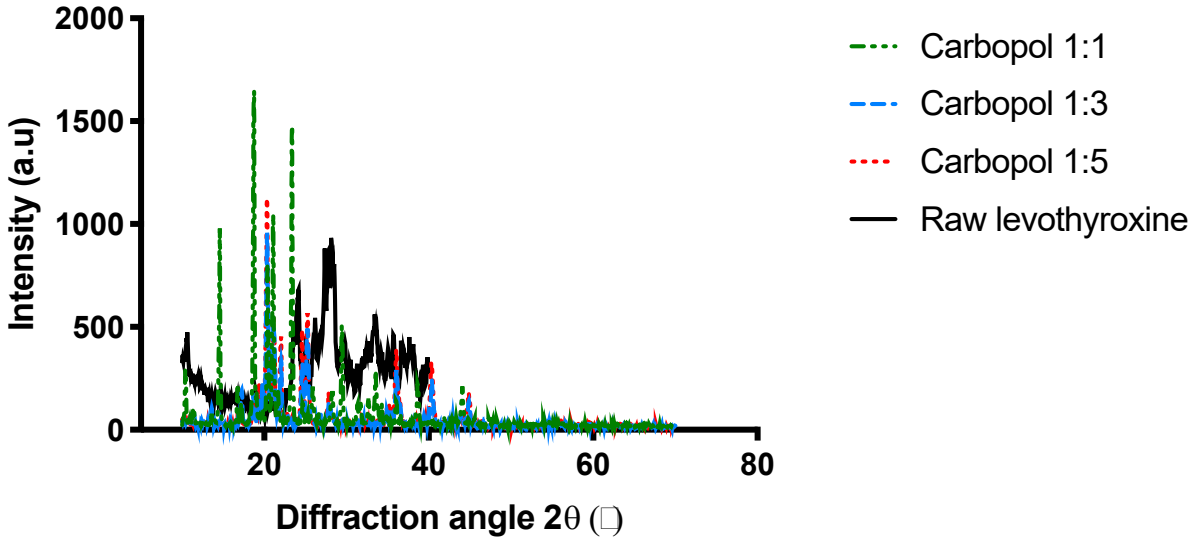

Figure 11. X-ray diffraction patterns of carbopol 1:1, carbopol 1:3, carbopol 1:5, and raw levothyroxine. X-rays were generated with a Cu-K_a source (1.00 Å). The intensity of the patterns is expressed in arbitrary units (y-axis).

4.6.2 PXRD for Polycarbophil-Levothyroxine Formulation

The X-ray diffraction patterns of levothyroxine powder and polycarbophil formulations are presented in Figure 12. The polycarbophil 1:1 formulation had five major peaks at 2θ angle 14.3°, 19.3°, 20.7°, 22.0°, and 23.9°. The minor peaks for polycarbophil 1:1 occurred at 10.0° and 17.0°, 29.0°, 36.0°, and 44.0°. Only one major peak at 15.9° was detected for the polycarbophil 1:3 formulation. However, several minor peaks appeared at 17.4°, 20.1°, 31.4°, and 35.4°. The only major peak for the polycarbophil 1:5 formulation was at 20.8°, while the minor peaks occurred at 36.2°, 40.5°, and 45.1°.

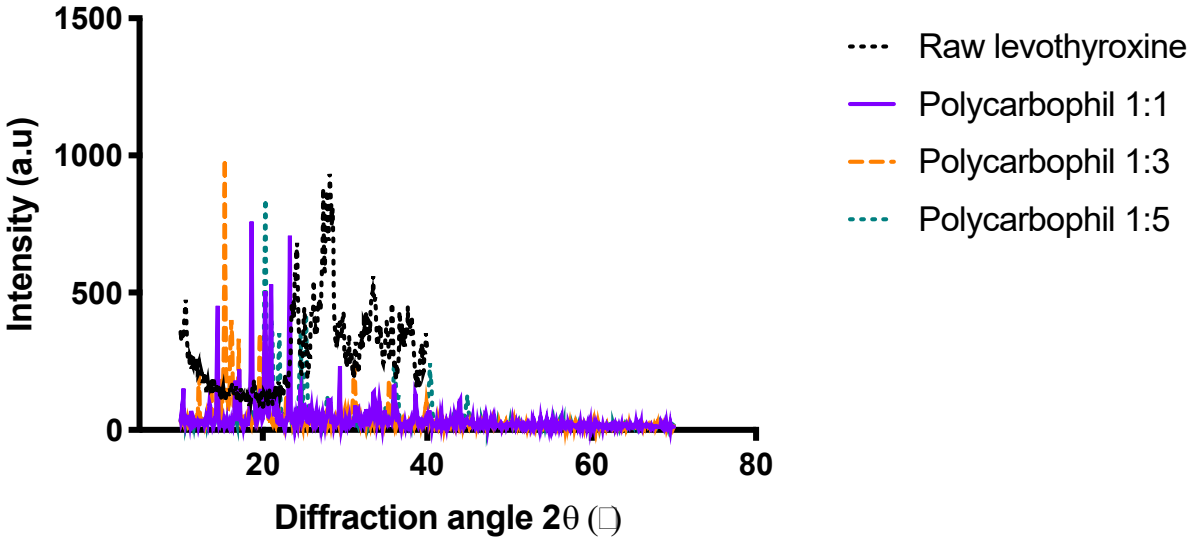

Figure 12. X-ray diffraction patterns of polycarbophil 1:1, polycarbophil 1:3, polycarbophil 1:5, and raw levothyroxine. X-rays were generated with a Cu-K_a source (1.00 Å). The intensity of the peak is expressed in arbitrary units (y-axis).

4.6.3 PXRD for Levothyroxine-HPMC Formulation

Similar to the other formulations, levothyroxine-HPMC formulations diffracted x-rays at specific 2θ angles. The HPMC 1:1 formulation showed difrraction at two major angles, 19.3° and 20.5°; the minor diffraction peaks occurred at 22.1°, 25.3°, 25.4°, 36.2°, and 40.5° (Figure 13). The only major peak that appeared in the HPMC 1:3 formulation was at 20.3°. Minor peaks for the HPMC 1:3 formulations were detected at 22.8°, 25.4°, 27.9°, 36.2°, 40.6°, and 45.1°(Figure 13). HPMC 1:5 had only one major peak, which was at 20.8°. The minor peaks for HPMC 1:5 were similar to those obtained from the HPMC 1:3 formulation; the peaks occurred at 22.5°, 25.4°, 27.4°, 36.0°, 40.6°, and 45.0° (Figure 13).

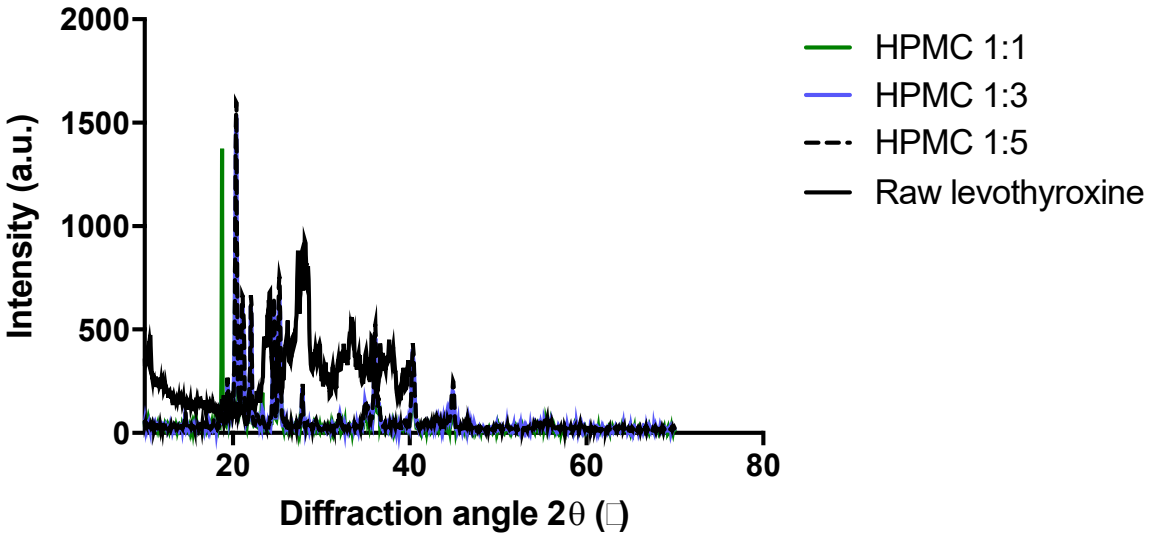

Figure 13. X-ray diffraction patterns of HPMC 1:1, HPMC 1:3, HPMC 1:5, and raw levothyroxine. X-rays were generated with a Cu-K_a source (1.00 Å). The intensity of the formulation is expressed in arbitrary units (y-axis).

4.6.4 PXRD for Levothyroxine-Chitosan Formulation

The chitosan 1:1 formulation had a major diffraction peak at 19.3°. The minor peaks for chitosan 1:1 appeared at 21.1° and 21.3°, 24.2°, 25.9°, and 36.2° (Figure 14). The only major peak for HPMC 1:3 formulation appeared at 21.1°. Most of the minor peaks for HPMC 1:3 were clustered between 20° and 30°. However, two distinct small peaks occurred at 36.4° and 40.9°. The HPMC 1:5 formulation presented only one major peak at 21°. The minor peaks for the HPMC 1:5 were clustered between 20° and 30°.

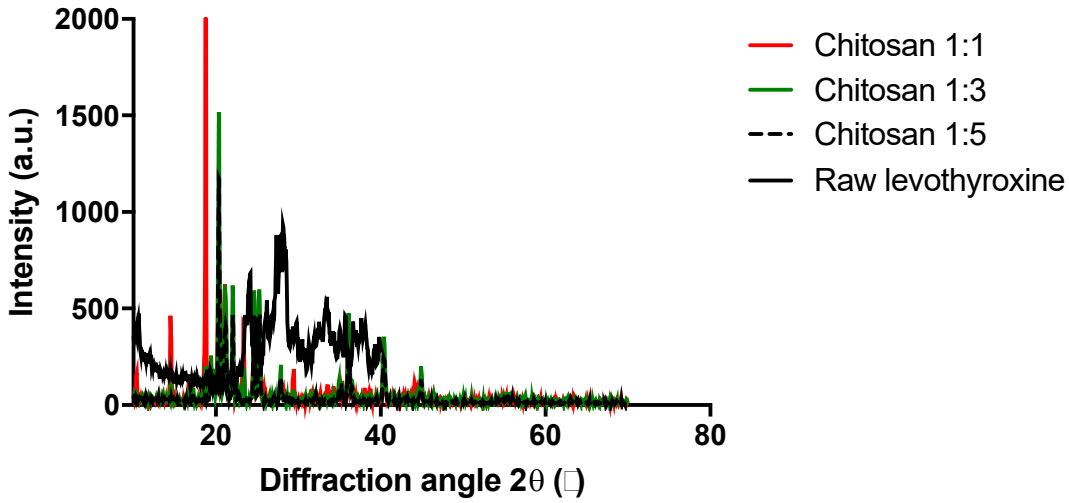

Figure 14. X-ray diffraction patterns of chitosan 1:1, chitosan 1:3, chitosan 1:5, and raw levothyroxine. X-rays were generated with a Cu-Ka source (1.00 Å). The intensity of the patterns is expressed in arbitrary units (y-axis).

4.7 *In vitro* Drug Release

4.7.1 *In vitro* Release of Levothyroxine-Carbopol Formulations

There was a significant difference in the amount of levothyroxine released from the 1:1 formulation compared to the 1:3 (two-way ANOVA: $p<0.05$) and 1:5 (two-way ANOVA: $p<0.05$) formulations (Figure 15). However, there was no significant difference in the percentage of levothyroxine released from 1:1 and 1:3 after three hours (two-way ANOVA: $p>0.05$). The amount of levothyroxine released from carbopol 1:3 was not significantly from carbopol 1:5 (two-way ANOVA $p<0.05$). At 1.5 hours, carbopol 1:1 formulation had 100.0 ± 4.8 % mean cumulative release of levothyroxine. However, carbopol 1:3 and 1:5 at 1.5 hours had a mean cumulative release of 53.0 ± 9.7 % and 24.2 ± 7.3 % respectively. Carbopol 1:3 formulations reached 92.5 ± 8.1 % mean cumulative

release at 3 hours. The maximum mean cumulative percentage of levothyroxine released from carbopol 1:5 was 66.5 ± 3.2 % over 4 hours.

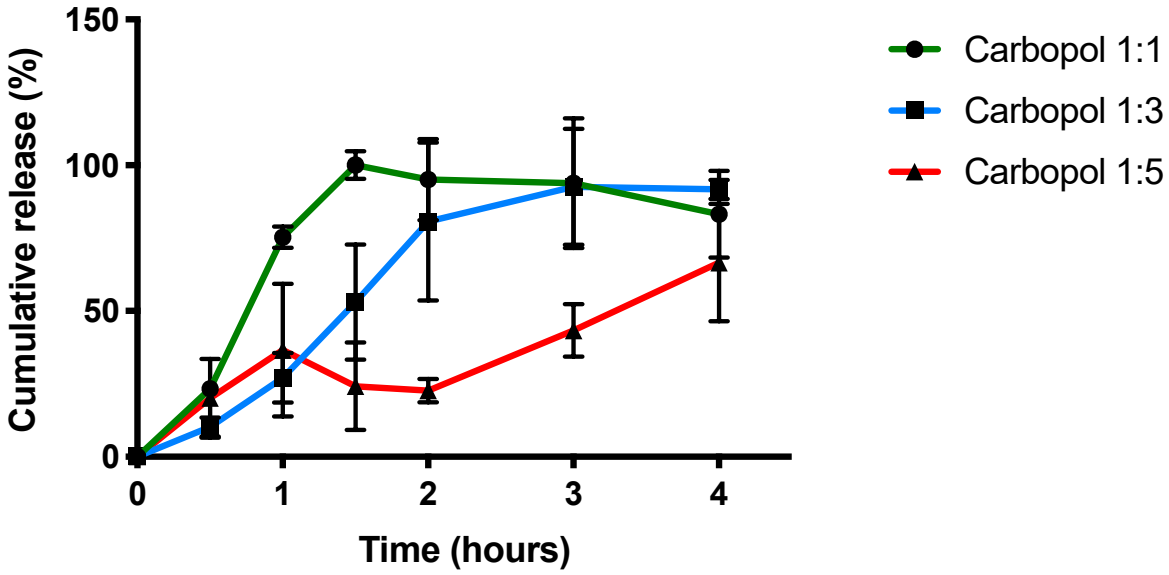

Figure 15. *In vitro* cumulative release of levothyroxine from carbopol 1:1, carbopol 1:3, and carbopol 1:5 formulations. Samples were withdrawn from the Franz diffusion receptor chamber at different time intervals over 4 hours (0.5, 1, 1.5, 2, 3, 4 hours). The volume of samples withdrawn at each time point was 0.5 ml. The data represents the mean ± SD (n=3).

4.7.2 *In vitro* Profile of Levothyroxine-Polycarbophil Formulations

The cumulative percentage release of levothyroxine from polycarbophil 1:1, 1:3, and 1:5 is shown in Figure 16. A significantly different amount of levothyroxine was released from the 1:1 formulation compared to the 1:5 (two-ANOVA: $p<0.05$). Also, the percentage of levothyroxine released from 1:3 differed significantly from the 1:5 after one hour (two-ANOVA: $p>0.05$). The 1:3 formulation released 92.9 ± 3.1 % of levothyroxine at the 1.5-hour time point. Polycarbophil 1:1 achieved 92.8 ± 2.3 % release

at 3 hours. At the four-hour time point, no significant difference was found in the amount of levothyroxine released from polycarbophil 1:1, 1:3, and 1:5 (two-way ANOVA: $p>0.05$). After 2 hours, the polycarbophil 1:5 formulation showed a linear trend until it reached the four-hour time point. The maximum cumulative release (%) achieved by the 1:5 formulation was 84.2 ± 6.0 %. Polycarbophil 1:1, 1:3, and 1:5 at 1.5 hours had a mean cumulative release of 78.0 ± .6 %, 92.9 ± 3.1 %, and 42.7 ± 8.0 %, respectively.

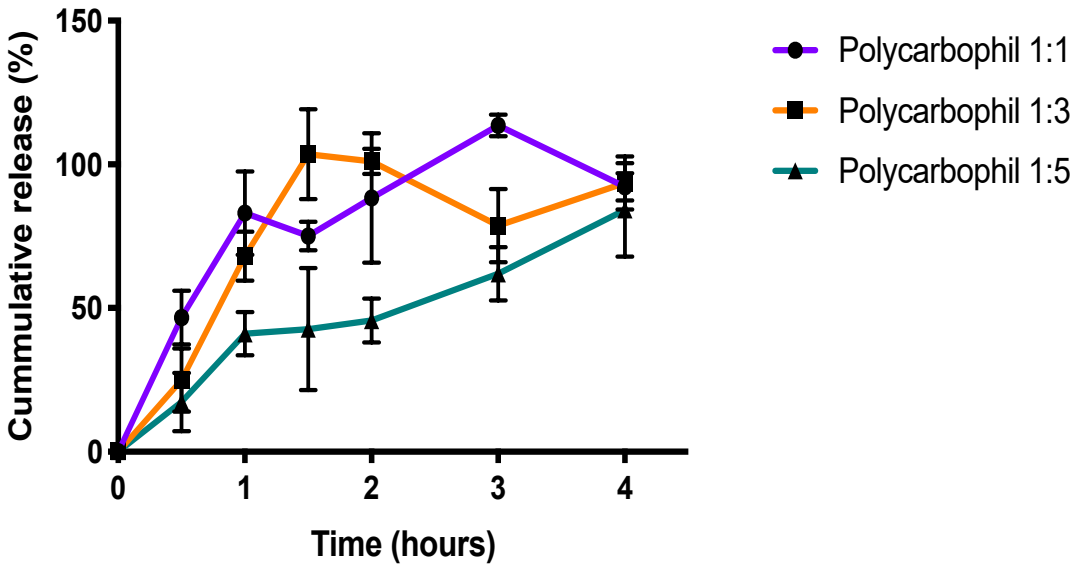

Figure 16. *In vitro* cumulative release of levothyroxine from polycarbophil 1:1, polycarbophil 1:3, and polycarbophil 1:5 formulations. Samples were withdrawn from the Franz diffusion receptor chamber at different time intervals over 4 hours (0.5, 1, 1.5, 2, 3, 4 hours). The volume of samples withdrawn at each time point was 0.5 ml. The quantity of samples removed at each time point was 0.5 ml. The data represents the mean ± SD (n=3).

4.7.3 *Invitro* Release of Levothyroxine-HPMC Formulations

The percentage of levothyroxine released from any of the HPMC formulations before 1.5 hours did not significantly differ (two ANOVA: $p>0.05$). However, after 1.5

hours the amount of levothyroxine released from the 1:3 formulation was significantly different from the 1:1 formulation (two-way ANOVA: $p<0.05$) and 1:5 formulation (two-way ANOVA: $p<0.05$). Also, the amount of levothyroxine released from HPMC 1:3 did not significantly differ compared to HPMC 1:1 (two-way ANOVA: $p<0.05$). At 1.5 hours, HPMC 1:1, 1:5 both had 68.08 ± 6.7 % and 78.17 ± 7.7 % (Figure 17). The mean cumulative release of levothyroxine-HPMC 1:3 formulation had 94.69 ± 4.8 % at 1.5 hours. HPMC 1:3 achieved 96.3 ± 2.2 % levothyroxine release at 4 hours. HPMC 1:1 showed maximum release, 76.6 ± 3.7 % at 4 hours (Figure 17).

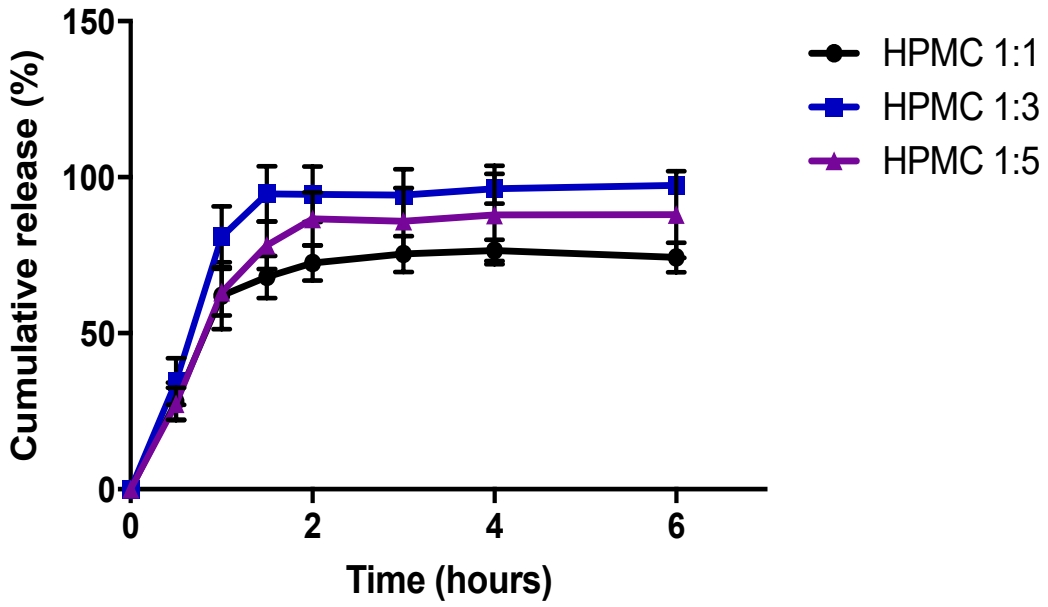

Figure 17. *In vitro* cumulative release of levothyroxine from HPMC 1:1, HPMC 1:3, and HPMC 1:5 formulations. Samples were withdrawn from the Franz diffusion receptor chamber at different time intervals over 6 hours (0.5, 1, 1.5, 2, 3, 4, 6 hours). The volume of samples withdrawn at each time point was 0.5 ml. The volume of samples withdrawn at each time point was 0.5 ml. The data represents the mean ± SD (n=3).

4.7.4 *Invitro* Release of Levothyroxine-Chitosan Formulations

Figure 18 shows the cumulative percentage release of levothyroxine from chitosan 1:1, 1:3, and 1:5. At 1.5 hours chitosan 1:1 and 1:3 formulations, both had 74.01 ± 4.2 % and 74.36 ± 3.2 % mean percent cumulative release of levothyroxine. The amount of levothyroxine released from the 1:1 formulation compared to the 1:3 and 1:5 formulations did not differ significantly (two-way ANOVA: $p>0.05$). However, there was a significant difference in the cumulative percentage of levothyroxine released from chitosan 1:5 compared to 1:1 and 1:3 at the one-hour and 1.5-hour time points (two-way ANOVA: $p>0.05$). The maximum mean cumulative release achieved by the 1:1, 1:3, and 1:5 was 74.01 ± 8.3 %, 76.6 ± 6.5 %, and 89.27 ± 4.4 %, respectively. After four hours, the drug release from the three formulations was 63.0 %. At that point (4 hours), no significant difference was measured in the percentage of levothyroxine release (two-way ANOVA: $p>0.05$).

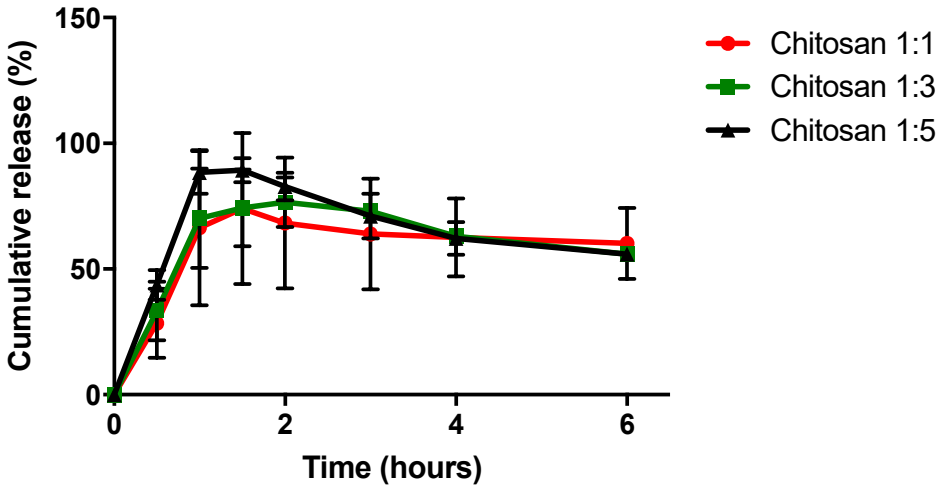

Figure 18. *In vitro* cumulative release of levothyroxine from chitosan 1:1, chitosan 1:3, and chitosan 1:5 formulations. Samples were removed from the Franz diffusion receptor chamber at different time intervals over 6 hours (0.5, 1, 1.5, 2, 3, 4, 6 hours). The volume of samples removed at each time point was 0.5 ml. The amount of samples removed at each time point was 0.5 ml. The data represents the mean ± SD (n=3).

4.8 In vitro Release Kinetics

The mathematical models in Table 8 describe levothyroxine release from different polymers. The carbopol formulations 1:1, 1:3, and 1:5 followed Hixon-Crowell, Korsmeyer-Peppas, and first-order release mechanism, respectively. Interestingly, levothyroxine release from polycarbophil-based formulations depends on the drug: polymer ratio. At a ratio of 1:1, the Hixon-Crowell release pattern was observed. In contrast, at 1:3 and 1:5 combinations, the Higuchi model release pattern was apparent. Levothyroxine in HPMC 1:1 correlated with the Hixon-Crowell model, while HPMC 1:3 and 1:5 both displayed the Higuchi release pattern. A high correlation with the Hixon-Crowell and Korsmeyer-Peppas model was observed with the chitosan 1:1, chitosan 1:3, and chitosan 1:5 showed a Korsmeyer-Peppas release pattern.

Table 8. Mathematical models for levothyroxine release from carbopol, polycarbophil, HPMC, and chitosan. The squared correlation coefficient (R^2) was obtained from kinetic models based on the percent cumulative drug released.

	Higuchi (R^2)	**Zero Order (R^2)**	**First Order (R^2)**	**Hixon-Crowell (R^2)**	**Korsmeyer-Peppas (R^2)**
Carbopol 1:1	0.72	0.34	0.56	0.80	0.50
Carbopol 1:3	0.91	0.97	0.53	0.50	0.98
Carbopol 1:5	0.78	0.79	0.80	0.61	0.63
Polycarbophil 1:1	0.71	0.41	0.63	0.77	0.44
Polycarbophil 1:3	0.87	0.67	0.03	0.51	0.78
Polycarbophil 1:5	0.95	0.94	0.94	0.85	0.94
HPMC 1:1	0.76	0.49	0.76	0.85	0.49
HPMC 1:3	0.74	0.46	0.71	0.73	0.50
HPMC 1:5	0.88	0.53	0.83	0.87	0.58
Chitosan 1:1	0.52	0.25	0.29	0.55	0.34

	Higuchi (R^2)	**Zero Order (R^2)**	**First Order (R^2)**	**Hixon-Crowell (R^2)**	**Korsmeyer-Peppas (R^2)**
Chitosan 1:3	0.44	0.17	0.47	0.45	0.66
Chitosan 1:5	0.48	0.06	0.14	0.12	0.94

CHAPTER 5 DISCUSSION

Although most hypothyroid patients can be effectively treated using oral tablets, thyroid hormone management remains challenging for patients that cannot absorb oral levothyroxine [60]. Based on therapeutic, economic, and patient-acceptability perspectives, alternative levothyroxine delivery approaches are needed for such hypothyroid patients.

The aim of this project was to develop and characterize different polymer-based alternatives for the nasal delivery of levothyroxine. The four mucoadhesive polymers used in this study (carbopol, polycarbophil, HPMC, and chitosan) are considered Generally Recognized as Safe (GRAS) excipients [61]. The formulations were developed by lyophilization, and the drug to polymer ratio of 1:1, 1:3, and 1:5 was found to be most common and effective based on previous studies on mucoadhesive carriers and active pharmaceutical agents [53–55].

The formulations were characterized to determine percentage yield, percentage drug loading, morphology, particle size, zeta potential, differential scanning calorimetry (DSC), powder X-ray diffraction, and *in vitro* drug release. These analyses examined the suitability of the formulations developed in this study as potential alternatives for the delivery of levothyroxine.

5.1 Analytical method development and validation

The validation of the analytical method was conducted to ensure that data obtained from this study were accurate and reliable. The high performance liquid chromatography (HPLC) showed sufficient linearity (Figure 2) and acceptable accuracy (Table 4). In

addition, the percentage levothyroxine recovery was within the ICH recommended range of 95 % - 105 % [62]. Furthermore, the repeatability and inter-day studies designed to assess the precision of the method confirmed the reproducibility of the assay method (CV < 5 %) for intra-day and inter-day precision studies (Table 5). Accuracy studies were conducted to determine the validity of the measurements of standard samples with known concentrations. The relative standard deviation was less than 1 %, which was also within the acceptance criteria limits for accuracy studies [63]. The analytical method was accurate and precise for the detection and quantification of levothyroxine. Thus, HPLC was used for sample analysis, and routine validation was conducted bi-weekly during the study to ensure the equipment was at peak performance.

5.2 Percentage Yield and Drug Loading

Percentage yield is the ratio of the actual amount of formuation to the theoretical amount used in making the formulation, expressed as a percentage. For the carbopol, polycarbophil, HPMC, and chitosan formulations the percentage yield was between 98.0 ± 1.4 % - 100.7 ± 1.3 %, 99.5 ± 2.1 % - 101.1 ± 2.3 %, 100.0 ± 0.8 % - 102.0 ± 0.6 %, and 99.6 ± 0.5 % - 102.0 ± 0.1 %, respectively (Table 6). The high yield from the different formulations is indicative of the efficiency of lyophilization as a drug processing method for dry powder formulations. The main disadvantage of lyophilization is that it requires several steps, and it is also time-consuming. Spray-drying is another powder processing technique that overcomes the challenges of freeze-drying. However, results from a study by Coucke et al. suggested that freeze-dried samples result in higher bioavailability compared to spray-dried formulations [64]. Besides, several reports showed that freeze-drying enhances dissolution and solubility of formulations [65,66]. In Table 3, the

formulations show high percentage yield and high levothyroxine loading percentage that are within the acceptable range for early drug development studies. The polymer ratio and efficiency of lyophilization both contributed to the high amount of levothyroxine loaded in the various polymers.

5.3 Surface Morphology

Surface morphology affects various characteristics of a particle, such as friability, dissolution, stability, and adhesion [67,68]. All the formulations in this study showed a rough surface morphology (Figure 3, Figure 4, Figure 5, and Figure 6). Particles with rough surface morphology have more contact points, thereby increasing the potential for adhesion in the nasal epithelium [69]. The benefits of an irregular surface morphology over smooth morphology is still unclear as there have been results that support the benefits of both smooth and rough surface morphologies [67,70]. The point of agreement in the literature is that each formulation requires an optimum level of surface roughness and that modifications to surface morphology can enhance the performance of nasal formulations [71]. Consequently, the formulations in this study have mucoadhesive properties not just because of the polymers, but also due to their surface roughness which will allow them to adhere to multiple points in the nasal epithelium.

5.4 Particle Size

The mean particle size of each formulation is presented in Table 4. The type of polymer significantly influenced the size of particles (two-way ANOVA: $p<0.05$). The mean particle size of the carbopol and polycarbophil formulations increased with the amount of added polymer (Table 7). HPMC 1:3 had a mean particle size of 0.22 ± 0.06

μm, while chitosan 1:3, with the same polymer ratio had a mean particle size of 2.76 ± 1.38 μm (Table 7). Unlike the polyacrylic acids (carbopol and polycarbophil), the particle size of HPMC and chitosan formulations did not increase as the amount of polymer increased. (Table 7). However, the mean particle size was consistent within the polymer, supporting the finding that polymer type influenced particle size (Table 7). Heng et al. demonstrated that increasing particle size improved drug release up to a critical threshold [72]. Their results suggest that beyond the critical particle size threshold, an increase in particle size will not lead to more drug release. Generally, powder particles for nasal delivery fall within the range of 10 – 150 μm. This range ensures that particles remain in the nasal cavity and not deposited into the lungs [73]. However, particles that are less than 10 μm are usually preferred because they rapidly enter systemic circulation [74]. From Table 7, the formulations in this study have adequate particle size for nasal delivery.

5.5 Zeta Potential

The zeta potential of a formulation is a measure of the electrostatic repulsion between the particles [75]. Zeta potential plays an important role in the stability of powder formulations in a liquid media. Particles that are electronegative exert a repulsive force that prevents the particles from aggregating in a low liquid environment, like the mucous. Also, a formulation with high absolute zeta potential usually contains a very high total charge on its surface [76]. Generally, neutral particles have zeta potential between -10 mV and +10 mV, and formulations with a zeta potential lower than -30 mV are considered strongly anionic and exert strong repulsive force [77]. Table 7 shows that the most negatively charged formulations were derived from carbopol and polycarbophil

mucoadhesive polymers. The carbopol 1:1 formulation had a zeta potential of -52.4 ± 2.6 mV, and the polycarbophil 1:1 had a zeta potential of -40.5 ± 1.9 mV. In contrast, the most charged HPMC and chitosan formulations had -11.66 ± 3.16 mV (HPMC 1:1) and -19.17 ± 1.01 mV (chitosan 1:5). A possible explanation for the high negative charge on carbopol and polycarbophil is that both polymers are polyacrylic acids that can be deprotonated at neutral pH [78]. HPMC, however, is a nonionic cellulose ether, and chitosan is a cationic polysaccharide. The chemical characteristics of HPMC and chitosan provide a reason for the relatively low zeta potential compared to the polyacrylic acids (carbopol and polycarbophil). Chitosan has several positively charged amino groups, and the HPMC does not dissociate in aqueous media [79]. Therefore, it is plausible that the negative charges carried by the HPMC and chitosan formulations are derived from the main excipient of the formulations, mannitol.

5.6 Differential Scanning Calorimetry (DSC)

Figure 7 - Figure 9 show the DSC thermograms for carbopol, polycarbophil, HPMC, and chitosan formulations. The endothermic peaks in the thermograms indicate the melting of the crystalline formulations. Although each formulation comprised of three main compounds (polymer, levothyroxine, and mannitol), the DSC curve (thermograms) for each formulation had only one melting peak. This observation suggests that the formulations are homogenous and that levothyroxine was completely loaded into the polymers. Furthermore, the endothermic peaks indicated that the atoms in the formulations have a crystalline configuration [80]. Generally, exothermic peaks are

associated with amorphous compounds, while endothermic peaks, like those seen in Figure 7 – Figure 9 indicate crystalline arrangement [80].

5.7 Powder X-ray Diffraction

The arrangement of the atoms in the formulation was analyzed using powder X-ray diffraction. In pXRD, the structure of a compound is determined by measuring the scattering pattern of high-frequency waves [81]. The diffraction patterns of the formulations are shown in Figure 11 – Figure 14. The pXRD results support the observation from the DSC analysis that the formulations in this study are arranged in a crystalline configuration. Therefore, the formulations are expected to maintain stablility and morphology while in storage [82].

5.8 *In vitro* Drug Release and Kinetics of *In vitro* Release

The cumulative *in vitro* release of levothyroxine from carbopol was highest in the 1:1 formulation (Figure 15). Similarly, the polycarbophil 1:1 formulation achieved the highest cumulative percent release within its group (Figure 16). Both carbopol 1:1 and polycarbophil 1:1 released levothyroxine more than 90 % in less than two hours. These results are consistent with the findings of studies conducted by Cho et al. and Ugwoke et al. [57,83]. At 1.5 hours, the carbopol 1:1 formulation already achieved a cumulative percent release of 100 .0 ± 4.8%. Carbopol 1:1 maintained a steady cumulative release that was above 80 % through the duration of the experiment. Although the release of levothyroxine from carbopol 1:5 did not exceed 70 %, it showed a linear increase from

two hours to four hours. The polycarbophil formulation 1:1 showed the highest cumulative percent drug release. At 1.5 hours, polycarbophil 1:1, 1:3, and 1:5 of 72. 8 ± 0.6 %, 92.9 ± 3.1 %, and 42.7 ± 8.0 %, respectively. However, at 3 hours, the cumulative percent release of polycarbophil 1:1 reached 92.8 ± 2.3 %.

The release of levothyroxine from HPMC and chitosan is shown in Figure 17 and Figure 18, respectively. The HPMC formulations showed the fastest levothyroxine release compared to the other mucoadhesive polymers (Figure 17). There was no significant difference in the cumulative percentage of levothyroxine released from the different HPMC formulations (1:1, 1:3, and 1:5) before 1 hour (two-way ANOVA: $p>0.05$). From 0 – 1 hour, the HPMC formulations showed a linear increase of cumulative percent levothyroxine released with time. However, at 1.5 hours, the cumulative release plateaued uniformly and maintained steady levothyroxine release for the duration of the experiment (Figure 17). The chitosan formulations also showed a steady drug release; however, release from the 1:5 formulation decreased between 1.5 hours to 4 hours. Both HPMC 1:3 and chitosan 1:3 had the highest cumulative release profile compared to the other formulations within their respective groups. Some studies have shown that release decreased as the amount of polymer increased (similar results were obtained in the carbopol and polycarbophil formulations) [54,80]. However, the HPMC and chitosan *in vitro* release results suggest that more polymer led to increasing levothyroxine release. The finding may partly be because of the dissolution enhancing effect of both HPMC and chitosan [84,85]. In addition, drug loading can affect drug release from mucoadhesive formulations [86]. In this study, the formulations with the highest drug loading showed the best release.

Overall, the formulations demonstrated a steady controlled drug release. Several polymers, including those in this study, have previously been shown to enable the steady controlled release of drugs [87–89]. The *in vitro* release kinetics model suggests carbopol formulations 1:1, 1:3, and 1:5 followed Hixon-Crowell, Korsmeyer Peppas, and first-order release mechanisms, respectively (Table 8). The polycarbophil, HPMC, and chitosan 1:1 formulation followed the Higuchi release mechanism. The other chitosan formulations (1:3 and 1:5) displayed Korsmeyer Peppas release.

CHAPTER 6 SUMMARY AND CONCLUSION

The objectives of this study were to develop and characterize intranasal mucoadhesive formulations for the delivery of levothyroxine. The levothyroxine formulations were developed using four polymers: carbopol, polycarbophil, HPMC, and chitosan. Each polymer was used to formulate three different levothyroxine-polymer nasal powder. The amount of levothyroxine used in each formulation was the same, but the amount of polymer varied by a ratio of 1:1, 1:3, and 1:5 (levothyroxine to polymer ratio). The formulations were evaluated for percentage yield, percentage drug loading, morphology, particle size, zeta potential, differential scanning calorimetry (DSC), powder X-ray diffraction, and *in vitro* drug release. All the formulations in this study shared these main characteristics: 1) high percentage yield, 2) acceptable percentage drug loading, 3) rough surface morphology, 4) negative zeta potential, 5) crystalline configuration, 6) endothermic enthalpy, and 7) sustained drug release. Although the type and amount of polymer affected the size of the particles, each formulations particle size was below 50 μm (which is within the recommended limit for nasal powder formulations).

Finally, the results of this study suggest that nasal levothyroxine-mucoadhesive powder formulations based on carbopol, polycarbophil, HPMC, and chitosan polymers can be used as alternatives to injection therapies if validated in randomized human studies.

REFERENCES

1. Sherwood L. The Thyroid Gland. In: *Human Physiology : From Cells to Systems, Ninth Edition*. Cengage Learning; 2015:537-538; 541; 524.

2. Tortora, Gerard J. BHD. *Principles of Anatomy and Physiology, 15th Edition*. Wiley; 2016. https://www.wiley.com/en-us/Principles+of+Anatomy+and+Physiology%2C+15th+Edition-p-9781119320647. Accessed April 13, 2020.

3. Taylor PN, Albrecht D, Scholz A, et al. Global epidemiology of hyperthyroidism and hypothyroidism. *Nat Rev Endocrinol*. 2018;14(5):301-316. doi:10.1038/nrendo.2018.18

4. Yang F, Teng W, Shan Z, et al. *Epidemiological Survey on the Relationship between Different Iodine Intakes and the Prevalence of Hyperthyroidism*. Vol 146. www.eje.org.

5. Clemens K, Payne W, Van Uum SHM. Central hypothyroidism. *Can Fam Physician*. 2011;57(6):677-680. http://www.ncbi.nlm.nih.gov/pubmed/21673213. Accessed December 2, 2019.

6. Golden SH, Robinson KA, Saldanha I, Anton B, Ladenson PW. Prevalence and incidence of endocrine and metabolic disorders in the united states: A comprehensive review. *J Clin Endocrinol Metab*. 2009;94(6):1853-1878. doi:10.1210/jc.2008-2291

7. ClinCalc DrugStats Database. https://clincalc.com/DrugStats/. Accessed April 13, 2020.

8. Slater S. The discovery of thyroid replacement therapy. Part 3: A complete transformation. *J R Soc Med*. 2011;104(3):100-106. doi:10.1258/jrsm.2010.10k052

9. Weissel M. Role of desiccated thyroid extracts in the treatment of hypothyroidism: an update. *Austrian J Clin Endocrinol Metab*. 2019;12(4):159-164. doi:10.1007/s41969-019-0071-x

10. Murray GR. Note on the Treatment of Myxoedema by Hypodermic Injections of an Extract of the Thyroid Gland of a Sheep. *Br Med J*. 1891;2(1606):796-797. doi:10.1136/bmj.2.1606.796

11. Mackenzie WG. A case of myxcedema treated with great benefit by feeding with fresh thyroid glands. *Br Med J*. 1892;2(1661):940-941. doi:10.1136/bmj.2.1661.940

12. Malinowski H. *Bioavailability/Bioequivalence Studies in Evaluation of New Levothyroxine Products*.

13. Levothyroxine | C15H11I4NO4 - PubChem. https://pubchem.ncbi.nlm.nih.gov/compound/Levothyroxine#section=Computed-Properties. Accessed April 13, 2020.

14. Benvenga S, Bartolone L, Squadrito S, Lo Giudice F, Trimarchi F. Delayed intestinal absorption of levothyroxine. *Thyroid*. 1995;5(4):249-253. doi:10.1089/thy.1995.5.249

15. Bach-Huynh T, Nayak B, … JL-TJ of, 2009 undefined. Timing of levothyroxine administration affects serum thyrotropin concentration. *academic.oup.com*. https://academic.oup.com/jcem/article-abstract/94/10/3905/2597179. Accessed August 7, 2019.

16. Ward LS. The difficult patient: drug interaction and the influence of concomitant diseases on the treatment of hypothyroidism. *Arq Bras Endocrinol Metabol*. 2010;54(5):435-442. doi:10.1590/s0004-27302010000500002

17. Carvalho GA de, Fighera TM. Effect of gastrointestinal disorders in autoimmune thyroid diseases. *Transl Gastrointest Cancer*. 2014;4(1):76-82.

18. Liwanpo L, Hershman JM. Conditions and drugs interfering with thyroxine absorption. *Best Pract Res Clin Endocrinol Metab*. 2009;23(6):781-792. doi:10.1016/j.beem.2009.06.006

19. Yao X, Forte JG. Cell Biology of Acid Secretion by the Parietal Cell. *Annu Rev Physiol*. 2003;65(1):103-131. doi:10.1146/annurev.physiol.65.072302.114200

20. Cone RA. Barrier properties of mucus. *Adv Drug Deliv Rev*. 2009. doi:10.1016/j.addr.2008.09.008

21. Diamond J. Anatomy of a Ritual. *Nat Hist*. 2001;110(6):16-20.

22. Hinchcliffe M, Illum L. Intranasal insulin delivery and therapy. *Adv Drug Deliv Rev*. 1999;35(2-3):199-234. doi:10.1016/S0169-409X(98)00073-8

23. Bartos C, Pallagi E, Szabó-Révész P, et al. Formulation of levodopa containing dry powder for nasal delivery applying the quality-by-design approach. *Eur J Pharm Sci*. 2018. doi:10.1016/j.ejps.2018.07.061

24. Ghori MU, Mahdi MH, Smith AM, Conway BR. Nasal Drug Delivery Systems: An Overview. *J Appl Pharm Sci*. 2011;1(3):34-44. doi:10.12691/ajps-3-5-2

25. Bitter C, Suter-Zimmermann K, Surber C. Nasal drug delivery in humans. *Curr Probl Dermatol*. 2011;40:20-35. doi:10.1159/000321044

26. Bhat M, Toledo-Velasquez D, Wang LY, Malanga CJ, Ma JKH, Rojanasakul Y. Regulation of Tight Junction Permeability by Calcium Mediators and Cell Cytoskeleton in Rabbit Tracheal Epithelium. *Pharm Res An Off J Am Assoc Pharm Sci*. 1993;10(7):991-997. doi:10.1023/A:1018906504944

27. Pearce SC, Al-Jawadi A, Kishida K, et al. Marked differences in tight junction composition and macromolecular permeability among different intestinal cell types. *BMC Biol*. 2018;16(1):19. doi:10.1186/s12915-018-0481-z

28. Gibson RE, Olanoff LS. Physicochemical determinants of nasal drug absorption. *J Control Release*. 1987;6(1):361-366. doi:10.1016/0168-3659(87)90089-7

29. Moghaddam FA, Atyabi F, Dinarvand R. Preparation and in vitro evaluation of mucoadhesion and permeation enhancement of thiolated chitosan-pHEMA core-shell nanoparticles. *Nanomedicine Nanotechnology, Biol Med*. 2009;5(2):208-215. doi:10.1016/j.nano.2008.09.006

30. Soliman GM, Zhang YL, Merle G, Cerruti M, Barralet J. Hydrocaffeic acid-chitosan nanoparticles with enhanced stability, mucoadhesion and permeation properties. *Eur J Pharm Biopharm*. 2014;88(3):1026-1037. doi:10.1016/j.ejpb.2014.09.003

31. Gu JM, Robinson JR, Leung SHS. Binding of acrylic polymers to mucin/epithelial surfaces: Structure-property relationships. *Crit Rev Ther Drug Carrier Syst*. 1988;5(1):21-67.

32. Morimoto K, Morisaka K, Kamada A. Enhancement of nasal absorption of insulin and calcitonin using polyacrylic acid gel. *J Pharm Pharmacol*. 1985;37(2):134-136. doi:10.1111/j.2042-7158.1985.tb05024.x

33. Ugwoke MI, Agu RU, Verbeke N, Kinget R. Nasal mucoadhesive drug delivery: Background, applications, trends and future perspectives. *Adv Drug Deliv Rev*. 2005;57(11):1640-1665. doi:10.1016/j.addr.2005.07.009

34. Saito S, Ainai A, Suzuki T, et al. The effect of mucoadhesive excipient on the nasal retention time of and the antibody responses induced by an intranasal influenza vaccine. *Vaccine*. 2016;34(9):1201-1207. doi:10.1016/j.vaccine.2016.01.020

35. Tanaka A, Furubayashi T, Tomisaki M, et al. Nasal drug absorption from powder formulations: The effect of three types of hydroxypropyl cellulose (HPC). *Eur J Pharm Sci*. 2017;96:284-289. doi:10.1016/j.ejps.2016.09.028

36. Qiang F, Shin H-J, Lee B-J, Han H-K. Enhanced systemic exposure of fexofenadine via the intranasal administration of chitosan-coated liposome. *Int J Pharm*. 2012;430(1-2):161-166. doi:10.1016/j.ijpharm.2012.04.007

37. Agu RU, Ugwoke MI. In situ and ex vivo nasal models for preclinical drug development studies. *Sect Title Pharm*. 2008;7(Drug Absorption Studies):112-134. doi:10.1007/978-0-387-74901-3_5

38. Varma MVS, Kapoor N, Sarkar M, Panchagnula R. Simultaneous determination of digoxin and permeability markers in rat in situ intestinal perfusion samples by RP-HPLC. *J Chromatogr B Anal Technol Biomed Life Sci*. 2004;813(1-2):347-352. doi:10.1016/j.jchromb.2004.09.047

39. Olivier JC, Djilani M, Fahmy S, Couet W. In situ nasal absorption of midazolam in rats. *Int J Pharm*. 2001;213(1-2):187-192. doi:10.1016/S0378-5173(00)00668-2

40. Dyer AM, Hinchcliffe M, Watts P, et al. Nasal delivery of insulin using novel chitosan based formulations: A comparative study in two animal models between simple chitosan formulations and chitosan nanoparticles. *Pharm Res*. 2002;19(7):998-1008. doi:10.1023/A:1016418523014

41. Yu S, Zhao Y, Wu F, et al. Nasal insulin delivery in the chitosan solution: In vitro and in vivo studies. *Int J Pharm*. 2004;281(1-2):11-23. doi:10.1016/j.ijpharm.2004.05.007

42. Gungor S, Okyar A, Erturk-toker S, Baktir G, Ozsoy Y. Ondansetron-loaded chitosan microspheres for nasal antiemetic drug delivery: an alternative approach to oral and parenteral routes. *J Am Diet Assoc*. 1997;97(4):411-412. doi:10.3109/03639040903517906

43. Chamanza R, Wright JA. A Review of the Comparative Anatomy, Histology, Physiology and Pathology of the Nasal Cavity of Rats, Mice, Dogs and Non-human Primates. Relevance to Inhalation Toxicology and Human Health Risk Assessment. *J Comp Pathol*. 2015;153(4):287-314. doi:10.1016/j.jcpa.2015.08.009

44. Parija S, Mandal J. Ethics of involving animals in research. *Trop Parasitol*. 2013;3(1):4. doi:10.4103/2229-5070.113884

45. Huh Y, Cho HJ, Yoon IS, et al. Preparation and evaluation of spray-dried hyaluronic acid microspheres for intranasal delivery of fexofenadine hydrochloride. *Eur J Pharm Sci*. 2010;40(1):9-15. doi:10.1016/j.ejps.2010.02.002

46. Agu RU, Jorissen M, Willems T, Augustijns P, Kinget R, Verbeke N. In-vitro nasal drug delivery studies: comparison of derivatised, fibrillar and polymerised collagen matrix-based human nasal primary culture systems for nasal drug delivery studies. *J Pharm Pharmacol*. 2001;53(11):1447-1456. doi:10.1211/0022357011777981

47. Dimova S, Brewster ME, Noppe M, Jorissen M, Augustijns P. The use of human nasal in vitro cell systems during drug discovery and development. *Toxicol Vitr*. 2005;19(1):107-122. doi:10.1016/j.tiv.2004.07.003

48. Reichl S, Becker K. Cultivation of RPMI 2650 cells as an in-vitro model for human transmucosal nasal drug absorption studies: Optimization of selected culture conditions. *J Pharm Pharmacol*. 2012;64(11):1621-1630. doi:10.1111/j.2042-7158.2012.01540.x

49. Ladel S, Schlossbauer P, Flamm J, Luksch H, Mizaikoff B, Schindowski K. Improved in vitro model for intranasal mucosal drug delivery: Primary olfactory and respiratory epithelial cells compared with the permanent Nasal cell line RPMI 2650. *Pharmaceutics*. 2019;11(8). doi:10.3390/pharmaceutics11080367

50. Sugibayashi K, Morimoto Y, Natsume H. Evaluation of Enhancers to Increase Nasal Absorption Using Ussing Chamber Technique. *Biol Pharm Bull*. 1994;17(2):316-322. doi:10.1248/bpb.17.316

51. Bruschi ML. Mathematical models of drug release. In: *Strategies to Modify the Drug Release from Pharmaceutical Systems*. Elsevier; 2015:63-86. doi:10.1016/B978-0-08-100092-2.00005-9

52. Jug M, Hafner A, Lovri´c JL, et al. An overview of in vitro dissolution/release methods for novel mucosal drug delivery systems. *J Pharm Biomed Anal*. 2018;147:350-366. doi:10.1016/j.jpba.2017.06.072

53. Belgamwar VS, Patel HS, Joshi AS, Agrawal A, Surana SJ, Tekade AR. Design and development of nasal mucoadhesive microspheres containing tramadol HCl for CNS targeting. *Drug Deliv*. 2011;18(5):353-360. doi:10.3109/10717544.2011.557787

54. Harikarnpakdee S, Lipipun V, Sutanthavibul N, Ritthidej GC. Spray-dried mucoadhesive microspheres: Preparation and transport through nasal cell monolayer. *AAPS PharmSciTech*. 2006;7(1):E79-E88. doi:10.1208/pt070112

55. Kılıçarslan M. The effect of the drug/polymer ratio on the properties of the verapamil HCl loaded microspheres. *Int J Pharm*. 2003;252(1-2):99-109. doi:10.1016/S0378-5173(02)00630-0

56. Lee MK, Kim MY, Kim S, Lee J. Cryoprotectants for freeze drying of drug nano-suspensions: Effect of freezing rate. *J Pharm Sci*. 2009;98(12):4808-4817. doi:10.1002/jps.21786

57. Cho HJ, Balakrishnan P, Shim WS, Chung SJ, Shim CK, Kim DD. Characterization and in vitro evaluation of freeze-dried microparticles composed of granisetron-cyclodextrin complex and carboxymethylcellulose for intranasal delivery. *Int J Pharm*. 2010;400(1-2):59-65. doi:10.1016/j.ijpharm.2010.08.030

58. Collier JW, Shah RB, Bryant AR, Habib MJ, Khan MA, Faustino PJ. Development and application of a validated HPLC method for the analysis of dissolution samples of levothyroxine sodium drug products. *J Pharm Biomed Anal*. 2011;54(3):433-438. doi:10.1016/j.jpba.2010.08.025

59. Rojewska M, Bartkowiak A, Strzemiecka B, Jamrozik A, Voelkel A, Prochaska K. Surface properties and surface free energy of cellulosic etc mucoadhesive polymers. *Carbohydr Polym*. 2017. doi:10.1016/j.carbpol.2017.05.019

60. Vaidya B, Pearce SHS. Management of hypothyroidism in adults. *BMJ*. 2008;337(7664):284-289. doi:10.1136/bmj.a801

61. Bernkop-Schnürch A. *Oral Delivery of Macromolecular Drugs: Barriers, Strategies and Future Trends*. 2009th ed. Springer https://books.google.ca/books. Accessed June 23, 2020.

62. Collier JW, Shah RB, Bryant AR, Habib MJ, Khan MA, Faustino PJ. Development and application of a validated HPLC method for the analysis of dissolution samples of levothyroxine sodium drug products. *J Pharm Biomed Anal*. 2011. doi:10.1016/j.jpba.2010.08.025

63. ICH Official web site : ICH. https://www.ich.org/. Accessed June 26, 2020.

64. Coucke D, Vervaet C, Foreman P, Adriaensens P, Carleer R, Remon JP. Effect on the nasal bioavailability of co-processing drug and bioadhesive carrier via spray-drying. *Int J Pharm*. 2009;379(1-2):67-71. doi:10.1016/j.ijpharm.2009.06.008

65. Shamma RN, Basha M. Soluplus®: A novel polymeric solubilizer for optimization of Carvedilol solid dispersions: Formulation design and effect of method of preparation. *Powder Technol*. 2013. doi:10.1016/j.powtec.2012.12.038

66. Badr-Eldin SM, Elkheshen SA, Ghorab MM. Inclusion complexes of tadalafil with natural and chemically modified β-cyclodextrins. I: Preparation and in-vitro evaluation. *Eur J Pharm Biopharm*. 2008;70(3):819-827. doi:10.1016/j.ejpb.2008.06.024

67. Flament MP, Leterme P, Gayot A. The influence of carrier roughness on adhesion, content uniformity and the in vitro deposition of terbutaline sulphate from dry powder inhalers. *Int J Pharm*. 2004;275(1-2):201-209. doi:10.1016/j.ijpharm.2004.02.002

68. Burnett DJ, Heng JYY, Thielmann F, Garcia AR, Naderi M, Acharya M. Measuring surface roughness of pharmaceutical powders using vapor sorption methods. *AAPS PharmSciTech*. 2011;12(1):56-61. doi:10.1208/s12249-010-9571-0

69. Kawashima Y, Serigano T, Hino T, Yamamoto H, Takeuchi H. Effect of surface morphology of carrier lactose on dry powder inhalation property of pranlukast hydrate. *Int J Pharm*. 1998;172(1-2):179-188. doi:10.1016/S0378-5173(98)00202-6

70. Kaialy W. On the effects of blending, physicochemical properties, and their interactions on the performance of carrier-based dry powders for inhalation — A review. *Adv Colloid Interface Sci*. 2016;235:70-89. doi:10.1016/j.cis.2016.05.014

71. Peng T, Lin S, Niu B, et al. Influence of physical properties of carrier on the performance of dry powder inhalers. *Acta Pharm Sin B*. 2016;6(4):308-318. doi:10.1016/j.apsb.2016.03.011

72. Heng PWS, Chan LW, Easterbrook MG, Li X. Investigation of the influence of mean HPMC particle size and number of polymer particles on the release of aspirin from swellable hydrophilic matrix tablets. *J Control Release*. 2001;76(1-2):39-49. doi:10.1016/S0168-3659(01)00410-2

73. Marx D, Williams G, Birkhoff M. Intranasal Drug Administration-An Attractive Delivery Route for Some Drugs. 2015. doi:10.5772/59468

74. Donovan MD, Huang Y. Large molecule and particulate uptake in the nasal cavity: The effect of size on nasal absorption. *Adv Drug Deliv Rev*. 1998;29(1-2):147-155. doi:10.1016/S0169-409X(97)00066-5

75. Bhattacharjee S. DLS and zeta potential - What they are and what they are not? *J Control Release*. 2016;235:337-351. doi:10.1016/j.jconrel.2016.06.017

76. Tao W, Zeng X, Liu T, et al. Docetaxel-loaded nanoparticles based on star-shaped mannitol-core PLGA-TPGS diblock copolymer for breast cancer therapy. *Acta Biomater*. 2013;9(11):8910-8920. doi:10.1016/j.actbio.2013.06.034

77. Clogston JD, Patri AK. Zeta potential measurement. *Methods Mol Biol*. 2011;697:63-70. doi:10.1007/978-1-60327-198-1_6

78. Khutoryanskiy V V. Advances in Mucoadhesion and Mucoadhesive Polymers. *Macromol Biosci*. 2011. doi:10.1002/mabi.201000388

79. Lee CA, Kim BS, Cho CW. Quantitative evaluation of mucoadhesive polymers to compare the mucoadhesion. *J Pharm Investig*. 2016. doi:10.1007/s40005-016-0233-4

80. Alhalaweh A, Andersson S, Velaga SP. Preparation of zolmitriptan-chitosan microparticles by spray drying for nasal delivery. *Eur J Pharm Sci*. 2009. doi:10.1016/j.ejps.2009.07.003

81. De Rossi AC, De Lima VA. Processed Drug Classification and Temporal Analysis by Technical Chemometrics for Quality Controlling Using Spectroscopy of FT-IR and X-Ray Diffraction. *Orbital Electron J Chem*. 2018;10(7). doi:10.17807/orbital.v10i7.1138

82. Shah HS, Chaturvedi K, Hamad M, Bates S, Hussain A, Morris K. New Insights on Solid-State Changes in the Levothyroxine Sodium Pentahydrate during Dehydration and its Relationship to Chemical Instability. *AAPS PharmSciTech*. 2019;20(1):39. doi:10.1208/s12249-018-1264-0

83. Ugwoke MI, Exaud S, Van Den Mooter G, Verbeke N, Kinget R. Bioavailability of apomorphine following intranasal administration of mucoadhesive drug delivery systems in rabbits. *Eur J Pharm Sci*. 1999;9(2):213-219. doi:10.1016/S0928-0987(99)00061-5

84. Riekes MK, Kuminek G, Rauber GS, De Campos CEM, Bortoluzzi AJ, Stulzer HK. HPMC as a potential enhancer of nimodipine biopharmaceutical properties via ball-milled solid dispersions. *Carbohydr Polym*. 2014;99:474-482. doi:10.1016/j.carbpol.2013.08.046

85. Gavini E, Hegge AB, Rassu G, et al. Nasal administration of Carbamazepine using chitosan microspheres: In vitro/in vivo studies. *Int J Pharm*. 2006;307(1):9-15. doi:10.1016/j.ijpharm.2005.09.013

86. Hasçiçek C, Gönül N, Erk N. Mucoadhesive microspheres containing gentamicin sulfate for nasal administration: Preparation and in vitro characterization. *Farmaco*. 2003;58(1):11-16. doi:10.1016/S0014-827X(02)00004-6

87. Ugwoke MI, Sam E, Van Den Mooter G, Verbeke N, Kinget R. Nasal mucoadhesive delivery systems of the anti-parkinsonian drug, apomorphine: Influence of drug-loading on in vitro and in vivo release in rabbits. *Int J Pharm*. 1999. doi:10.1016/S0378-5173(99)00018-6

88. Ishikawa T, Watanabe Y, Takayama K, Endo H, Matsumoto M. Effect of hydroxypropylmethylcellulose (HPMC) on the release profiles and bioavailability of a poorly water-soluble drug from tablets prepared using macrogol and HPMC. *Int J Pharm*. 2000;202(1-2):173-178. doi:10.1016/S0378-5173(00)00426-9

89. Bartkowiak A, Rojewska M, Hyla K, Zembrzuska J, Prochaska K. Surface and swelling properties of mucoadhesive blends and their ability to release fluconazole in a mucin environment. *Colloids Surfaces B Biointerfaces*. 2018. doi:10.1016/j.colsurfb.2018.09.014